Literature Study for the Master's Thesis

Modeling of Immiscible Incompressible Turbulent Two-Phase Stratified Pipe Flow

Berkcan Kapusuzoğlu

April 11, 2016

Contents

Summary

The work described in this report is the literature survey part of the master thesis project "Modeling of immiscible incompressible turbulent two-phase stratified pipe flow". The literature survey is focused on the current state-of-the-art of modeling turbulent two-phase stratified flow. This report meant to identify and validate the most suitable candidate model for inclusion in the multiphase flow models that are being developed in the Scientific Computing group of the Delft Institute for Applied Mathematics. For that reason, experiments that have been carried out in the Laboratory for Aero- and Hydrodynamics of Faculty of Mechanical, Maritime and Materials Engineering of Delft University of Technology are used together with the results of (Eggels, 1994). The algorithm developed in the Scientific Computing group is based on a specific version of the Mass-Conserving Level Set (MCLS) method, which is the starting point of this thesis. This algorithm is going to be improved with necessary boundary conditions for discretization of the equations that describe immiscible incompressible two-phase flow in a circular pipe geometry.

In this report, three different turbulence models, standard $k - \epsilon$ model, Reynolds Stress Model (RSM), and Large Eddy Simulation (LES), are introduced. Direct Numerical Simulation (DNS) and LES are chosen to estimate the computational resources for single-phase pipe flow test case with friction Reynolds number of 395. In section 4, the physics of stratified two-phase flow is described and the importance of representing the interface between two immiscible phases to obtain conservation of mass is explained in section 6. In order to develop a three-dimensional numerical model for immiscible two-phase pipe flow, cylindrical coordinates are used to obtain a boundary-fitting grid. In section 6, the MCLS method, which combines the Level Set (LS) method and the Volume of Fluid (VOF) method, is described in order to conserve mass while representing the interface.

The turbulence model that can be used for this study depends mainly on the available computational resources of the Scientific Computing group. Accordingly, problem complexities of different models are analyzed in detail. Estimating problem complexity (i.e., the number of total grid points required) for single-phase turbulent flow gives a rough estimate for the number of unknowns and an inference about the complexity of two-phase flow. The comparison of computational costs showed that DNS is possible for two-phase stratified pipe flow test case only for low Reynolds numbers. For high Reynolds number flows, DNS is not feasible and LES is considered to be the promising technique since the computational resources required for DNS becomes excessive. Therefore, LES needs to be investigated elaborately for turbulent two-phase stratified pipe flow test case.

1 Introduction

Any flow that consists of more than one fluid or a fluid and a solid is called a *multiphase flow*. Multiphase flow can be classified according to the state of different phases such as gas and liquid flow, liquid and solid flow or gas and particle flow. If the state or the phase are the same, but the material properties are different (i.e. oil and water; liquid-liquid) for the flow, then the flow is also classified as a multiphase flow.

In general, multiphase flow has two general topologies: *disperse flow* and *separated flow*. Disperse flow consists of particles, drops or bubbles in the flow. However, in separated flow, as the name suggests, the streams of different fluids are separated by interfaces.

Almost every process technology has involvement with multiphase flow, thus, it occurs in many areas in industry, such as oil and gas recovery, (nuclear) power generation, food and chemical production. For safe transport and processing, the multiphase flow is required to be stable and predictable. Therefore, computational fluid dynamics (CFD) plays an important role at this point to simulate the environment and find the most cost-effective and efficient system design.

For many two-phase flow applications, the fluids flow in a single pipeline configuration. In long distance pipelines (e.g. steam and water or natural gas and oil flows), in power generation, petrochemical and process plants, the flow regime is so called stratified flow (Fig. 1a). With an increase in the flow rate, waves occur on the interface of the two fluids. The stratified flow in the pipeline first changes to stratified wavy flow (Fig. 1b), then to slug flow (Fig. 1c), as the gas velocity increases. If necessary precautions are not taken, these waves can get high enough to reach the top of the pipe. After that point, the gas flow can be blocked and the flow becomes discontinuous, which leads to formation of slugs. This should be avoided at all times since it can lead to pressure fluctuations and damage in the pipeline system; especially at the bends. Therefore, being able to predict the onset of the transition from wavy to slug flow is very important.

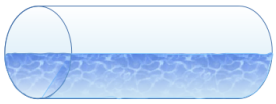

(a) Stratified flow

(b) Stratified wavy flow

(c) Slug flow

Figure 1: Gas-liquid flow regimes in horizontal pipes.

In this study, modeling of immiscible incompressible *turbulent* two-phase stratified flow is investigated. The aim of this thesis is to make a start with turbulence modeling for stratified two-phase flow. Different models are used and compared in order to find the most appropriate model, which predicts the onset of instability of the interface and the

formation of slugs. The main challenge for modeling turbulent two-phase flow is the turbulent conditions for bulk motion. Turbulence plays an important role in the transition of stratified flow to wavy flow. Moreover, waves on the interface have an influence on the dynamics of the interface, which leads to turbulence. Therefore, modeling turbulent two-phase flow is difficult compared to modeling turbulent single phase flow. There are quite a few turbulent models have been developed for turbulent single phase flow. However, not all of these models are extended to turbulent two-phase flow. Hence, models for turbulent two-phase flow are still not well established as models for single phase flow.

Turbulence models for turbulent incompressible single-phase flow are assessed in section 3 in order to compare computational cost and accuracy of different models before assessing the turbulent incompressible immiscible stratified two-phase flow in section 5. This way an insight is obtained for the number of unknowns required to model the flow and for the two-phase case, which is similar to the single-phase in terms of wall and inlet-outlet boundary conditions, and the inner region flow regime. The minimum computational cost that is possible with the *large eddy simulation (LES)* method for the single-phase flow is calculated in section 3 to be able to make inferences about the two-phase case, and to decide how to proceed with the turbulent two-phase flow modeling. In particular, DNS and LES are investigated carefully, especially, near-wall treatment and at the interface in order to realize and decrease the computational cost of the problem.

In the Laboratory for Aero- and Hydrodynamics of Faculty of Mechanical, Maritime and Materials Engineering of Delft University of Technology, experiments have been performed to predict the formation of slugs and the transition from laminar to turbulent flow. The configuration and flow parameters of the experiments are used in this thesis, and the results of the thesis are validated with the results of the experiments. Moreover, the computational technique used in the work of Eggels (1994) (e.g., grid estimation procedure) is compared in Appendices A and B with the methodology that is used in this thesis. In that manner, the model can be validated and limitations of all models can be identified clearly.

In this thesis, first, single phase flow is going to be simulated with DNS and then, if possible, two-phase flow will be simulated with DNS. It is feasible to use DNS to simulate two-phase flow within a reasonable amount of time with the available computational resources since the Reynolds number [1] is low enough. For this reason, DNS is going to be used to compare the results with experiments. However, the computational cost of DNS increases rapidly for high Reynolds number flows and the available resources in the Scientific Computing group of the Delft Institute for Applied Mathematics is not enough to simulate a high Reynolds number two-phase flow with DNS. Therefore, LES is realized as the most promising technique for turbulent two-phase flow.

[1] $Re = uL/\nu$ is the Reynolds number, u is the mean velocity of the fluid, L is the characteristic length scale of the flow geometry (e.g., the pipe diameter), and ν is the kinematic viscosity of the fluid.

2 Problem Description

When the flow becomes turbulent due to the high velocities of the fluids, it becomes challenging to model the turbulent behavior near the interface correctly. The turbulent flow near the interface affects the momentum transfer between the phases, which is the critical and peculiar phenomenon of turbulent two-phase flows.

Although, stratified flow is considered to be the simplest case for gas-liquid flow, it is not completely understood. The difficult part is the formation of waves at the interface and the interaction between this deformed interface and the two fluids. Experimental studies have been carried out for stratified wavy gas-liquid flow. However, it is quite challenging to get an accurate result for the velocity profile close to the interface (Vallée et al., 2008).

In order to solve the Navier-Stokes equations for turbulent flow, equations should be formulated. Pressure and velocity of a fluid, which are governed by Navier-Stokes equations, can be decomposed into mean and fluctuating parts Eq. (7) with *Reynolds decompostion* [2]. The continuity and the Navier-Stokes equations can be described only with the mean value by taking average of the Eqs. (9) and (10) in time. As a result of averaging, the *Reynolds Averaged Navier-Stokes (RANS)* equations are obtained and new unknown terms, *Reynolds stresses* appear in the equations, which need to be modeled (see Eq. (13)). This leads to a *closure problem*, which means that the number of unknowns is larger than the number of equations. Moreover, when new equations are developed for these unknown terms, more unknown terms appear in the equations. In fact, the closure problem suggests that there is a need for infinite number of equations in order to describe the turbulence statistically.

Numerical methods for solving the governing equations and the closure problem for turbulent two-phase flow are quite complex. In most of the cases, two-phase flows show oscillatory behavior and requires to solve costly transient problem (Ghorai and Nigam, 2006). The waves on the interface have an effect of changing the flow from laminar to turbulent. The turbulent fluctuations in two phases will influence the dynamics of the interface.

For single-phase flow, different turbulence models can be used for specific type of problems. However, it is not that straightforward to use turbulence models for turbulent two-phase flow since the momentum transfer at the interface cannot be handled easily (Ghorai and Nigam, 2006). The most common numerical approach for single-phase turbulent flow used in engineering applications is based on the RANS equations (see Eq. (11)), in which the effect of turbulence fluctuations are modeled. This approach yields different models, such as two-equation models ($k - \epsilon$ model), which can be used to predict many flows that are fully turbulent except flows with strong separation, swirling, or rotation. Another model that rises from the application of Reynolds averaging is the Reynolds Stress Model (RSM), which can be used for free shear flows with strong anisotropy, flows with sudden changes in the mean strain rate.

Direct numerical simulation (DNS) is the most accurate and easy-to-implement numerical approach to the solution of turbulent flow. In DNS, all of the scales of turbulent motion

[2] A mathematical technique that decomposes the instantaneous quantities into time-averaged and fluctuating quantities.

are resolved in space and time explicitly. The range is from macro-structure scales (energy-carrying) to micro-structure scales (dissipative motions), which makes DNS a very costly method. The number of grid points is proportional to the $Re^{9/4}$ (see Eq. (1)). Therefore, DNS is applicable only to simple geometries, and is limited to the flows with low Reynolds numbers. It is often used to validate the results of other turbulence models together with experiment results.

In LES, only the dissipative motions, the micro-structures, are modeled and the rest of the motions are resolved. It simulates the problem with a reasonable accuracy, which is comparable to the accuracy of the DNS with less computational effort. LES can be used for flows having the effect of irrotational strains and normal stress due to being isotropic.

In the experiment, a circular pipe, which has a diameter of 0.05 m and a length of 10 m, has two fluids flowing at ambient pressure and temperature. Each of the phases flow through the pipe with a different viscosity and density. The flow characteristics are determined by the shear stresses and gravity, which are affecting the interface and flow near the walls. When the flow rate is at a moderate level, the effect of gravity is observed on the flow, i.e. the stratification occurs and the phase with the higher density flow through the bottom region and the phase with the lower density flow through the top region. Both fluids are assumed to be incompressible and separated by an interface. The flow becomes fully developed over a length of 7.5 m.

There can be fluctuations at the interface between two phases when the gas flow rate increases, though, the liquid layer is fully laminar. For air and water this occurs when the air phase becomes turbulent; $Re_{air} \approx 3500$. The water phase is turbulent when $Re_{water} \approx 3400$. The Reynolds number Re is defined as $Re_f = u_f D_{fh}/\nu_f$, where u_f is the bulk velocity of the fluid, D_{fh} is the hydraulic diameter, and ν_f is the kinematic viscosity of the fluid. In air phase, $D_{gh} = 4A_g/(S_{wg} + S_{int})$, and in water phase $D_{lh} = 4A_l/S_{wl}$, where A_g and A_l are the cross-sectional areas respectively for gas and liquid phases, and S_{wg}, S_{wl}, and S_{int} are the wetted perimeters [3]. For the turbulent non-wavy stratified case (intermittency factor ∼0.99; which is the fraction of time that motion is turbulent) the Reynolds number is ∼3400. The friction Reynolds number [4] for the single phase pipe flow is $Re_\tau = 395$ (Birvalski, 2015).

The grid-point requirements for DNS of single phase channel flow, N_{DNS}, is (Wilcox et al., 1998)

$$N_{DNS} \sim (3Re)^{9/4}. \tag{1}$$

Even for the single phase case that has relatively low Reynolds number, the computational cost of DNS is large. For the two-phase case with $Re_{water} \approx 3400$, the computational cost is even larger.

The grid-point requirements for LES of single phase channel flow can be estimated with

[3] The wetted perimeter is the length of the total surface in contact with the fluid. For a single-phase pipe flow, the wetted perimeter is equal to πD, where D is the diameter of the pipe.

[4] It is defined as the ratio of inner (close to the wall) and outer length scales (further away from the wall), $Re_\tau = u^*\delta/\nu = \delta/\delta_\nu$, where u^* and δ_ν are defined in Eqs. (22) and (23) respectively, and δ represents the outer layer length scale for the flow.

respect to the requirement of DNS (Wilcox et al., 1998)

$$N_{LES} \approx \left(\frac{0.4}{Re_{\tau}^{1/4}} \right) N_{DNS}. \tag{2}$$

The number of grid points required for numerical simulation varies when using wall-modeled and wall-resolved LES. These different approaches of LES are discussed in more detail in the subsection 3.3.

The object of this study is to distinguish the advantages of turbulent models by getting more insight into the current state-of-the-art of modeling turbulent two-phase stratified flow. The results from an experiment, which has been carried out in the Laboratory for Aero- and Hydrodynamics of Faculty of Mechanical, Maritime and Materials Engineering of Delft University of Technology, are used to validate the results of this study (Birvalski, 2015). The main aim of this master thesis is to simulate the flow in this experiment and compare measured and computed velocity profiles. The main difficulty to resolve the flow is the feasibility of performing such a simulation using either DNS, LES or another turbulence model for turbulent two-phase flow.

In this thesis, LES is found to be applicable from a computational point of view. However, it is not known how to model the momentum transfer between gas and liquid phases, which is very crucial. In order to validate this work, results of this study should be as close as possible to the results of the experiment that includes the effect of momentum transfer between the phases. First, the computational cost and accuracy of DNS and LES in single-phase flow need to be analyzed. After analyzing the single-phase pipe flow with DNS and LES and checking the feasibility of LES for the turbulent two-phase flow, the immiscible incompressible turbulent two-phase stratified flow is going to be modeled with LES, in which the momentum transfer between the phases is initially going to be ignored because of the fact that there is not a robust method to simulate turbulent two-phase stratified flow and to make the problem slightly easier.

3 Introduction to Turbulence Modeling for Single-Phase Flow

Turbulent flow is three dimensional, chaotic, diffusive, quasi-random, dissipative and intermittent. In turbulent flow, the field parameters are not steady, but random functions of space and time and are characterized by velocity fluctuations in all directions. The tensor notation (in particular, the Einstein summation convention [5]) of conservation equation of mass for an incompressible fluid with constant viscosity is:

$$\frac{\partial u_i}{\partial x_i} = 0, \tag{3}$$

where u and p are velocity and pressure fields respectively. The flow is governed by incompressible Navier-Stokes equations and the conservation equation for momentum:

$$\rho \frac{\partial u}{\partial t} + \rho \frac{\partial}{\partial x_j}(u_j u_i) = -\frac{\partial p}{\partial x_i} + \frac{\partial}{\partial x_j}(2\mu s_{ij}) + g, \tag{4}$$

where ρ, μ, s_{ij} and g are the density, viscosity, strain-rate tensor and gravity respectively. The strain-rate tensor is as follows:

$$s_{ij} = \frac{1}{2}\left(\frac{\partial u_i}{\partial x_j} + \frac{\partial u_j}{\partial x_i}\right). \tag{5}$$

Together with the continuity Eq. (3), the equations of motion can be written as:

$$\rho \frac{\partial u}{\partial t} + \rho u_j \frac{\partial u_i}{\partial x_j} = -\frac{\partial p}{\partial x_i} + \mu \frac{\partial^2 u_i}{\partial x_i \partial x_j} + g. \tag{6}$$

The Navier-Stokes equations are non-linear and difficult to solve analytically. The exact solution can be obtained only by doing simplifications, which are usually not realistic. Therefore, it is hard to get more insight into the nature of turbulence by analytically solving these equations.

Due to the large computational resources required to resolve the flow at the appropriate length and time-scale, there is a need to model the equations. The need to model additional equations for the new unknown terms is called *Turbulence Modeling*. These are the turbulence models based on Reynolds Averaged Navier-Stokes (RANS) equations (time averaged) in the order of increasing complexity:

- Algebraic (zero equation) models: mixing length (first order model),
- One equation models: k-model, ν_t-model (first order model),
- Two equation models: $k - \epsilon$, $k - \omega^2$ (first order model),
- Algebraic stress models: ASM (second order model),
- Reynolds stress models (second order model).

[5] In Einstein summation convention, subscripted variables only appear twice in any term, and these subscripted variables are assumed to be summed over. It is used to simplify expressions including summations of vectors, matrices, and tensors.

In this study, $k - \epsilon$ and Reynolds stress models are investigated together with DNS and LES. DNS and LES are analyzed more elaborately than other models for single-phase turbulent pipe flow.

DNS, in which all details of the flow are resolved, is not feasible for high Reynolds number flows. However, for moderate Reynolds number flows its results can be used to validate the results of turbulence models, and it is also used to identify the physical processes involved in the problem.

In LES, the computational cost is smaller than DNS but larger than Reynolds stress models. Large scales are resolved and the small scales of the flow are modeled accordingly. For large fluctuating flows, LES is expected to be more reliable and accurate than Reynolds stress models (e.g. flow over bluff bodies, which has unsteady separation and vortex shedding (Pope, 2001)).

At the end of each section, the properties of different methods are summarized and their limitations are discussed and compared.

3.1 Reynolds Averaged Navier-Stokes (RANS)

3.1.1 Two Equation Model: $k - \epsilon$

In order to solve turbulent flow, it is considered to be statistically stationary, which means the joint probability distribution - which represents the likelihood of occurrence of two events at the same time and together (i.e. the probability of event x occurring at the same time with event y) - of the flow does not change when time is shifted. As a result, the mean and variance of the flow parameters are constant over time and do not have a pattern. By this means, the velocity field u_i and the pressure field p can be decomposed into a mean (time-averaged) and fluctuating part:

$$u_i = \overline{u_i} + u_i^{'}, \quad p = \overline{p} + p^{'}. \tag{7}$$

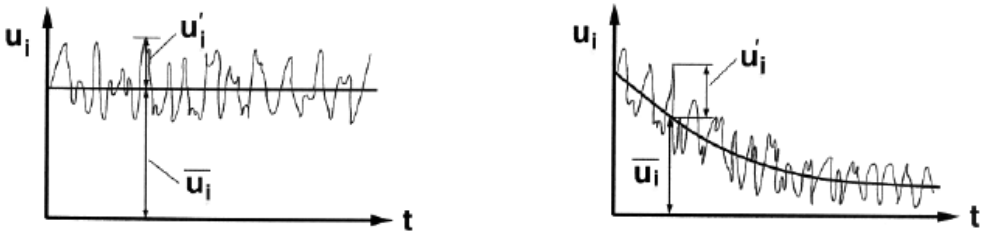

(a) Statistically stationary (b) Statistically unsteady

Figure 2: Statistically stationary flows, where u_i:=instantaneous velocity, $\bar{u}_i$:=mean velocity (time-averaged velocity), and $u_i^{'} := u_i - \overline{u}_i$:=velocity fluctuation.

The aim is to obtain set of equations to describe the average properties of the turbulent flow. The time average is defined as:

$$\overline{f} = \lim_{T\to\infty} \frac{1}{T} \int_{t_0}^{t_0+T} f dt. \tag{8}$$

Introducing the decomposition (7):

$$\rho \left[\frac{\partial(\overline{u_i} + u_i^{'})}{\partial t} + (\overline{u_j} + u_j^{'}) \frac{\partial(\overline{u_i} + u_i^{'})}{\partial x_j} \right] = -\frac{\partial(\overline{p} + p^{'})}{\partial x_i} + \mu \frac{\partial^2(\overline{u_i} + u_i^{'})}{\partial x_j \partial x_j}, \tag{9}$$

$$\frac{\partial(\overline{u_i} + u_i^{'})}{\partial x_i} = 0. \tag{10}$$

Applying the decomposition (i.e. the flow is statistically stationary, Fig. 2a) and the rules of averaging, the following Reynolds Averaged Navier-Stokes (RANS) equations are obtained:

$$\rho \left[\frac{\partial \overline{u}_i}{\partial t} + \overline{u_j} \frac{\partial \overline{u}_i}{\partial x_j} \right] = -\frac{\partial \overline{p}}{\partial x_i} + \frac{\partial}{\partial x_j} \left(\mu \frac{\partial \overline{u}_i}{\partial x_j} - \rho \overline{u_i^{'} u_j^{'}} \right), \tag{11}$$

$$\frac{\partial(\overline{u_i} + u_i^{'})}{\partial x_i} = 0. \tag{12}$$

However, application of the Reynolds decomposition leads to new unknowns, which are called Reynolds stresses and turbulent fluxes. The Reynolds stress tensor is defined as:

$$\tau_{ij} := \rho\overline{u_i' u_j'}. \tag{13}$$

In Newtonian fluids, the molecular shear stress is given by: $\tau_{ij}^{mol} = -\mu_T \left[\frac{\partial \overline{u_i}}{\partial x_j} + \frac{\partial \overline{u_j}}{\partial x_i}\right] = -2\mu\overline{S_{ij}}$, where $\overline{S_{ij}}$ is the mean-rate of strain tensor. By using the turbulent-viscosity hypothesis (Boussinesq), the deviatoric (anisotropic) Reynolds stress $\left(\rho\overline{u_i' u_j'} - \frac{2}{3}\rho k\delta_{ij}\right)$ is proportional to the mean rate of strain (Avila, 2015):

$$\tau_{ij}^{RANS,a} = \rho\overline{u_i' u_j'} - \frac{2}{3}\rho k\delta_{ij} = -\mu_T \left[\frac{\partial \overline{u_i}}{\partial x_j} + \frac{\partial \overline{u_j}}{\partial x_i}\right] = -2\rho\nu_T \overline{S_{ij}}, \tag{14}$$

where a in the superscript refers to the anisotropic part of Reynolds stress, and $\nu_T(\vec{x}, t)$ is the turbulent viscosity. Thus, the momentum equation is as follows:

$$\frac{\partial \overline{u}_i}{\partial t} + \overline{u}_j \frac{\partial \overline{u}_i}{\partial x_j} = -\frac{1}{\rho}\frac{\partial}{\partial x_i}(\overline{p} + \frac{2}{3}\rho k) + \frac{\partial}{\partial x_j}\left[\nu_{eff}\left(\frac{\partial \overline{u}_i}{\partial x_j} + \frac{\partial \overline{u}_j}{\partial x_i}\right)\right], \tag{15}$$

where $\nu_{eff} = \nu + \nu_T(\vec{x}, t)$. By specifying $\nu_T(\vec{x}, t)$, which is not a constant (since a constant do not change the same equation with the same unknowns), the closure problem is solved (instead of $\overline{p}$ and k, $q = \overline{p} + \frac{2}{3}\rho k$ is only used) (Avila, 2015).

The $k - \epsilon$ model is investigated since it is the most widely used turbulence model and included in all commercial CFD codes. It can be summarized as follows:

1. RANS + turbulent-viscosity hypothesis: $\nu_T = l^* u^*$,
2. Velocity scale: $u^* \propto \sqrt{k}$,
3. Length scale: $l^* \propto k^{3/2}/\epsilon$,
4. Turbulent viscosity is defined by $\nu_T = C_\mu k^2/\epsilon, C_\mu = 0.09$,
5. The RANS are solved for $\overline{u}(\vec{x})$, $\overline{p}(\vec{x})$, together with
6. Model equations for $k(\vec{x})$ and $\epsilon(\vec{x})$,

A transport equation for the turbulent kinetic energy $k = \frac{1}{2}\overline{u_i' u_i'}$ can be derived as follows:

- Subtract the RANS from the Navier-Stokes equations to obtain transport equation for the fluctuation velocity field u_j',
- Take the dot product of the following equation with u_j':

$$\frac{\partial k}{\partial t} + \overline{u_i}\frac{\partial k}{\partial x_i} + \frac{\partial T_i'}{x_i} = P - \epsilon \quad \longrightarrow \quad \frac{\overline{D}k}{\overline{D}t} + \nabla \cdot T_i' = P - \epsilon, \tag{16}$$

$P := -\tau_{ij}^{RANS}\frac{\partial \overline{u_i}}{\partial x_j}$ is the production term,

$\epsilon := \nu\left(\overline{\frac{\partial u_i'}{\partial x_j}\frac{\partial u_i'}{\partial x_j}}\right)$ is the dissipation term,

$\vec{T'} := \frac{1}{2}\overline{u_i' u_j' u_j'} + \overline{\frac{p' u'_i}{\rho}} - \nu\frac{\partial k}{\partial x_i}$ is the energy flux term.

The dissipation and energy flux terms are unknown. Thus, these terms have to be modeled. The energy dissipation rate and energy flux terms are modeled respectively $\epsilon = C_D k^{3/2}/l_m$, $C_D = 0.08$, $T^{'} = -(\nu_T/\sigma_k)\nabla k$, $\sigma_k = constant = 1$. Boundary conditions for k can be imposed as Dirichlet at the inlet, Neumann at the outlet, zero at walls. Near the wall, the production term and the dissipation term are almost equal ($P \approx \epsilon$) (Avila, 2015).

The empirical equation for the dissipation (ϵ) is;

$$\frac{\overline{D}\epsilon}{\overline{D}t} = \nabla \cdot \left[\frac{\nu_T}{\sigma_\epsilon}\nabla\epsilon\right] + C_{\epsilon 1}\frac{P\epsilon}{k} - C_{\epsilon 2}\frac{\epsilon^2}{k}, \tag{17}$$

where the model constants can be determined by studying simple flows or by comparison with experimental data: $C_\mu = 0.09$, $C_{\epsilon 1} = 1.44$, $C_{\epsilon 2} = 1.92$, $\sigma_k = 1.0$, $\sigma_\epsilon = 1.3$ (Avila, 2015).

The implementation of $k - \epsilon$ model yields six variables; $\overline{u_1}$, $\overline{u_2}$, $\overline{u_3}$, $\overline{p}$, k, ϵ and six equations:

$$\frac{\overline{D}\overline{u_j}}{\overline{D}t} = \nabla \cdot [\nu_{eff}\nabla\overline{u_j}] - C_{\epsilon 1}\frac{P\epsilon}{k} - C_{\epsilon 2}\frac{\epsilon^2}{k}, \quad j = 1, 2, 3 \tag{18}$$

$$\nabla \cdot \overline{u_j} = 0, \tag{19}$$

$$\frac{\overline{D}k}{\overline{D}t} = \nabla \cdot \left[\frac{\nu_T}{\sigma_k}\nabla k\right] + P - \epsilon, \tag{20}$$

$$\frac{\overline{D}\epsilon}{\overline{D}t} = \nabla \cdot \left[\frac{\nu_T}{\sigma_\epsilon}\nabla\epsilon\right] + C_{\epsilon 1}\frac{P\epsilon}{k} - C_{\epsilon 2}\frac{\epsilon^2}{k}. \tag{21}$$

3.1.2 Wall Treatment

Viscous effect in the near-wall region is an important challenge in CFD. Modeling equation raises another challenge, which is how to resolve fluctuating flow parameters near-wall without using a very fine mesh.

In the presence of a solid wall, vorticity is generated and a turbulent boundary layer will occur. Close to the wall, the wall shear stress τ_w and the viscosity ν play an important role. This region is called the *viscous sublayer*, whereas the outer region, where large scale turbulent eddy shear dominates, is called the *outer layer*. In between these two layers, there exists an overlap layer called the *log-law region*, where velocity profile shows a logarithmic variation (see Fig. 3 and Fig. 4). In the viscous sublayer region, the effects of the pressure gradient and convection are assumed to be negligible. The important parameters in that region are density, viscosity, wall shear stress and normal distance from the wall. On the other hand, in the outer region, where the convection and pressure gradient are dominant, the effect of viscosity is assumed to be negligible.

In the near-wall region new parameters are defined that are called the *viscous scales* (Pope, 2001). A reference length scale (viscous length scale) and velocity scale (friction velocity) is defined as follows:

$$u^* = \sqrt{\frac{\tau_w}{\rho}}, \tag{22}$$

and the viscous length scale:

$$\delta = \nu\sqrt{\frac{\rho}{\tau_w}} = \frac{\nu}{u^*}. \tag{23}$$

These can be used to define a dimensionless velocity and a dimensionless length (wall unit) as:

$$u^+ := \frac{u}{u^*}, \tag{24}$$

$$y^+ := \frac{y}{\delta} = \frac{u^* y}{\nu}, \tag{25}$$

where u is the velocity component parallel to the wall, y is the distance normal to the wall, and ν is the kinematic viscosity of the fluid.

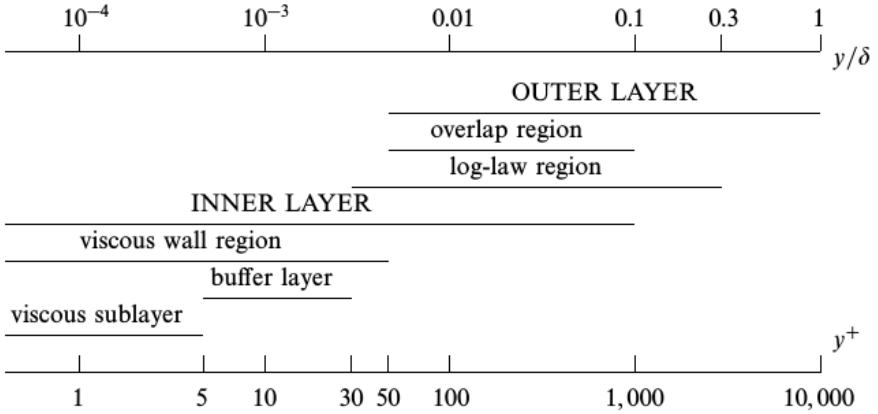

Figure 3: The law of the wall: layers defined in terms of y/δ for turbulent channel flow at $Re_\tau = 10^4$ (Pope, 2001).

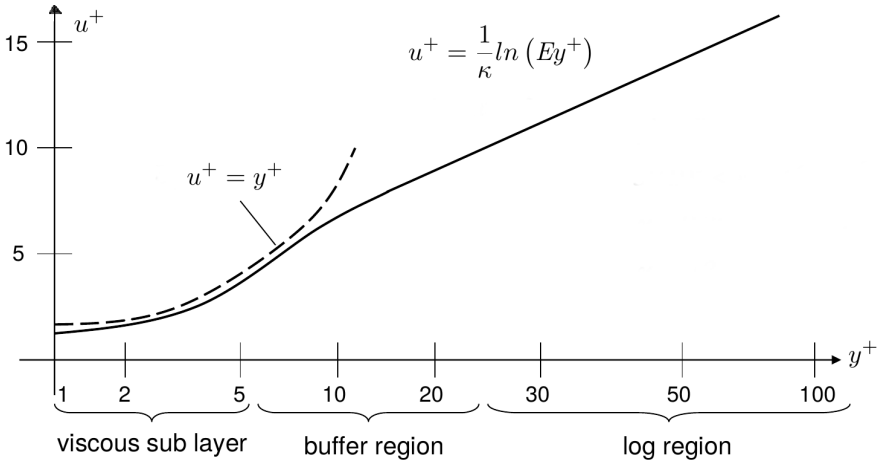

Figure 4: Near-wall mean velocity profiles, wall regions and layers.

The law of the wall defines that the average dimensionless velocity of a turbulent flow is proportional to the logarithm of the distance (dimensionless length or wall unit) from a certain point to the wall (Fig. 4).

The first layer is called the viscous sublayer (see Fig. 4) and at high Reynolds number the viscous sublayer is very thin ($y^+ < 5$). Thus, special near-wall treatments need to be applied. There are two possibilities for turbulence models in order to resolve the flow in the near-wall region; the low Reynolds number method, in which the mesh is very fine close to the wall, and the high Reynolds number method, in which *wall functions* are implemented. The second approach is less costly in terms of computations. However, important information about the physics of the problem is lost.

Over some region of the wall layer, viscous effects are large due to the no-slip boundary condition at the wall. These problems yield unsatisfactory results. In low Reynolds number, a way to overcome these problems is to introduce damping effects (Sondak, 1992).

Another option is to use wall functions, in which the flow in the near-wall region is modeled. By using wall functions, empirical laws are provided such that these laws make it possible to express the mean velocity parallel to the wall and turbulence parameters. Wall functions, which are based on the law of the wall and valid only in the log region, provide boundary conditions for the momentum and turbulent transport equations near the wall, instead of conditions at the wall itself. As a result, the viscous sublayer does not have to be resolved and the fluctuating flow parameters near the wall can be resolved without using a very fine mesh.

3.1.3 Wall Functions

It is important to model the flow in the near-wall region accurately because walls are the main source of vorticity and turbulence. Thus, in order to get an accurate result, wall functions or some other method should be used. In wall functions, the first point of the grid is assumed to be in the logarithmic layer and called y_p, which is an artificial parameter. The accuracy of the result depends on the choice of y_p. If the first grid-point is too close (i.e. located in the linear sublayer $y^+ < 5$), then the dimensionless velocity is equal to dimensionless length (Avila, 2015):

$$u^+ = y^+. \tag{26}$$

If the mean flow is parallel to the wall, then the log-law relations apply (log-law region: $y^+ > 30$) and the law of the wall for mean velocity yields (Sondak, 1992);

$$u^+ = \frac{1}{\kappa} ln\left(Ey^+\right), \tag{27}$$

where u^+ is the dimensionless velocity, κ is the von Kármán constant ≈ 0.41, E is an empirical constant $= 9.793$, and y^+ is the dimensionless length (Avila, 2015).

In the buffer layer, $5 < y^+ < 30$, none of the laws hold. Therefore, when $y^+ < 11$, linear approximation is more accurate, and when $y^+ > 11$, the logarithmic approximation is more accurate (Absi, 2009).

A no slip condition is imposed at the wall (i.e. $u \neq 0$). In order to set boundary conditions for k and ϵ at the grid-point adjacent to the wall, the friction velocity and the wall shear stress should be computed. Substituting Eqs. (25) and (26) into Eqs. (22) and (23) yields

(Pope, 2001):

$$\frac{u}{u^*} = \frac{1}{\kappa} ln \left(E \frac{u^* y}{\nu} \right), \tag{28}$$

for the log-law region, and

$$\frac{u}{u^*} = \frac{u^* y}{\nu}, \tag{29}$$

for the viscous sublayer (Sondak, 1992).

In the log region, production and dissipation of turbulent kinetic energy are almost equal $P \approx \rho\epsilon$. The production term for a simple two dimensional boundary layer, when the $y = x_2$ direction is normal to the wall, is $P := -\tau^t du/dy$ (Sondak, 1992), thus,

$$-\tau^t \frac{du}{dy} = \rho\epsilon. \tag{30}$$

The turbulent shear stress can also be expressed as:

$$\tau^t = \mu_t \frac{du}{dy} = C_\mu \rho \frac{k^2}{\epsilon} \frac{du}{dy}. \tag{31}$$

Solving this equation for ϵ, Eq. (17), by using Eqs. (24) and (29) yields the turbulent kinetic energy (Sondak, 1992):

$$k = \frac{(u^*)^2}{\sqrt{C_\mu}}, \tag{32}$$

where u^*_τ is the friction velocity and the dissipation is

$$\epsilon_p = \frac{(u^*)^3}{\kappa y_p}. \tag{33}$$

3.1.4 Realizable $k-\epsilon$ and other low-Re Turbulence Models

Realizable $k-\epsilon$ model uses the same turbulent kinetic energy equation as the standard $k-\epsilon$ model. However, the equation for ϵ is improved: A variable C_μ is used instead of a constant C_μ (Bakker, 2005).

The turbulent viscosity is $\nu_T = C_\mu k^2/\epsilon$, where:

$$C_\mu = \frac{1}{A_0 + A_s \frac{u^* k}{\epsilon}} \quad \textit{is now variable.} \tag{34}$$

A_0, A_s, and u^* are functions of velocity gradients.

This approach results in a new transport equation for the dissipation rate, ϵ:

$$\frac{\partial \epsilon}{\partial t} + \overline{u_j} \frac{\partial \epsilon}{\partial x_j} = \frac{\partial}{\partial x_j} \left[\left(\nu + \frac{\nu_t}{\sigma_\epsilon} \right) \frac{\partial k}{\partial x_j} \right] + C_{\epsilon 1} \frac{P\epsilon}{k} - C_{\epsilon 2} \frac{\epsilon^2}{k + \sqrt{\nu\epsilon}}. \tag{35}$$

Another model is the $k-\omega$ model, which was developed from the realization that most of the problems in $k-\epsilon$ model are due to the modeling of the ϵ equation. It is not easy to solve the ϵ equation since it has a local extremum close to the wall. In the $k-\omega$ model, the so-called turbulent frequency $\omega = \epsilon/k$ is used to replace the ϵ equation by a similar equation for ω. This gives rise to the $k-\omega$ model, which has a better accuracy near the wall but worse at free-stream.

3.1.5 Estimation of Unknown Parameters

Estimation of an initial condition for the turbulent kinetic energy is important to accurately predict flows, especially in high Reynolds number simulations.

$$k = \frac{3}{2}\left(\overline{u}I\right)^2, \tag{36}$$

where I is the (initial) turbulent intensity. Dissipation cannot be measured. It is generally modeled by:

$$\epsilon = \frac{k^{3/2}}{l^*}, \tag{37}$$

where l^* is the characteristic turbulent size.

3.1.6 Overview

Two additional equations need to be solved for the two turbulence quantities (i.e. k and ϵ) in the $k-\epsilon$ model of the RANS equations. By using these two quantities, a length scale ($l^* = k^{3/2}/\epsilon$), a velocity scale ($u^* = \sqrt{k}$), and turbulent viscosity ($\nu_T = C_\mu k^2/\epsilon$) are defined. Thus, the model is complete and flow dependent properties; such as $l_m(x)$, are not needed (Pope, 2001).

The $k-\epsilon$ model is the simplest complete turbulence model (computationally less expensive when used with wall functions). It is available in most of the commercial CFD packages, and has been used for different types of problems such as multiphase flows, heat transfer, and combustion. It can be accurate for simple flows, but it is usually inaccurate for complex flows (complex strain fields or substantial body forces, thin shear flows (McDonough, 2007)). The inaccuracy of the model comes from the turbulent-viscosity hypothesis and ϵ equation (Pope, 2001).

For specific types of problems, the wall treatment also should be modified to obtain correct results. In turbulent flow, wall treatment is very important. The wall have several effects on the flow:

- Low Reynolds number: the turbulence Reynolds number $Re_L := k^2/(\epsilon\nu)$ goes to zero as getting close to the wall,
- High shear rate: the highest mean shear rate $\partial u/\partial y$ is at the wall,
- Two-component turbulence: as the distance to the wall gets smaller, the turbulence becomes two-component, and
- Wall blocking.

Due to these effects of the wall, the standard $k-\epsilon$ turbulence model needs modifications to get an accurate result (Pope, 2001).

3.2 Reynolds Stress Model (RSM)

The *new* terms appearing in the RANS equations are modeled. The Reynolds Stress Model (RSM) directly solves for the Reynolds stresses $R_{ij} = \tau_{ij} = \rho\overline{u_i' u_j'}$ and for another

quantity that provides a length or time scale of the turbulence (e.g. turbulent dissipation ϵ). The main idea of the Reynolds stress model is that the stress tensor R_{ij} is calculated locally.

The Reynolds decomposed Navier-Stokes Eq. (9), contains information about the mean and instantaneous flow. By averaging this equation, the Reynolds Averaged Navier-Stokes equations Eq. (11) are obtained, which only have information about the mean flow behavior.

In order to get information about the instantaneous fluctuations, the RANS equations are subtracted from the decomposed Reynolds Navier-Stokes equations:

$$\rho\left[\frac{\partial u_i^{'}}{\partial t}+\overline{u_k}\frac{\partial u_i^{'}}{\partial x_k}+u_k^{'}\frac{\partial \overline{u}_i}{\partial x_k}+u_k^{'}\frac{\partial u_i^{'}}{\partial x_k}-\frac{\partial \overline{u_k^{'}u_i^{'}}}{\partial x_k}\right]=-\frac{\partial p^{'}}{\partial x_i}+\mu\frac{\partial^2 u_i^{'}}{\partial x_k\partial x_k}, \tag{38}$$

$$\frac{\partial(\overline{u_i}+u_i^{'})}{\partial x_i}=0. \tag{39}$$

Multiplying the i free index equation with $u_j^{'}$:

$$\rho\left[u_j^{'}\frac{\partial u_i^{'}}{\partial t}+\overline{u_j}u_k^{'}\frac{\partial u_i^{'}}{\partial x_k}+u_k^{'}u_j^{'}\frac{\partial \overline{u}_i}{\partial x_k}+u_j^{'}\frac{\partial u_k^{'}u_i^{'}}{\partial x_k}-u_j^{'}\frac{\partial \overline{u_k^{'}u_i^{'}}}{\partial x_k}\right]=-u_j^{'}\frac{\partial p^{'}}{\partial x_i}+\mu u_j^{'}\frac{\partial^2 u_i^{'}}{\partial x_k\partial x_k}. \tag{40}$$

Now multiply the other free index (i.e. j) with $u_i^{'}$:

$$\rho\left[u_i^{'}\frac{\partial u_j^{'}}{\partial t}+\overline{u_k}u_i^{'}\frac{\partial u_j^{'}}{\partial x_k}+u_i^{'}u_k^{'}\frac{\partial \overline{u}_j}{\partial x_k}+u_i^{'}\frac{\partial u_j^{'}u_k^{'}}{\partial x_k}-u_i^{'}\frac{\partial \overline{u_j^{'}u_k^{'}}}{\partial x_k}\right]=-u_i^{'}\frac{\partial p^{'}}{\partial x_j}+\mu u_i^{'}\frac{\partial^2 u_j^{'}}{\partial x_k\partial x_k}. \tag{41}$$

After adding Eqs. (40) and (41) together and averaging, the following equation for the Reynolds stress is obtained:

$$\begin{aligned}\frac{\partial \overline{u_i^{'}u_j^{'}}}{\partial t}+\overline{u_k}\frac{\partial \overline{u_i^{'}u_j^{'}}}{\partial x_k}=&-\overline{u_i^{'}u_k^{'}}\frac{\partial \overline{u_j}}{\partial x_k}-\overline{u_j^{'}u_k^{'}}\frac{\partial \overline{u_i}}{\partial x_k}-\frac{\partial}{\partial x_k}\overline{u_i^{'}u_j^{'}u_k^{'}}\\&-\frac{1}{\rho}\left[\overline{u_i^{'}\frac{\partial p^{'}}{\partial x_j}}+\overline{u_j^{'}\frac{\partial p^{'}}{\partial x_i}}\right]-2\nu\overline{\frac{\partial u_i^{'}}{\partial x_k}\frac{\partial u_j^{'}}{\partial x_k}}+\nu\frac{\partial^2\overline{u_i^{'}u_j^{'}}}{\partial x_k\partial x_k}.\end{aligned} \tag{42}$$

The pressure term in the right hand side can be simplified as follows:

$$-\frac{1}{\rho}\left[\overline{u_i^{'}\frac{\partial p^{'}}{\partial x_j}}+\overline{u_j^{'}\frac{\partial p^{'}}{\partial x_i}}\right]=-\frac{1}{\rho}\left(\frac{\partial\overline{p^{'}u_i}}{\partial x_j}+\frac{\partial\overline{p^{'}u_j}}{\partial x_i}\right)+\overline{\frac{p^{'}}{\rho}\left(\frac{\partial u_i}{\partial x_j}+\frac{\partial u_j}{\partial x_i}\right)}. \tag{43}$$

The first part of Eq. (43) is the transport part and the second part is the strain part of the velocity pressure gradient. By substituting these simplified expressions, the *Reynolds stress* equations are obtained:

$$\begin{aligned}\frac{\partial \overline{u_i^{'}u_j^{'}}}{\partial t}+\overline{u_k}\frac{\partial \overline{u_i^{'}u_j^{'}}}{\partial x_k}=&-\overline{u_i^{'}u_k^{'}}\frac{\partial \overline{u_j}}{\partial x_k}-\overline{u_j^{'}u_k^{'}}\frac{\partial \overline{u_i}}{\partial x_k}-\frac{\partial}{\partial x_k}\overline{u_i^{'}u_j^{'}u_k^{'}}-\frac{1}{\rho}\left(\frac{\partial\overline{p^{'}u_i^{'}}}{\partial x_j}+\frac{\partial\overline{p^{'}u_j^{'}}}{\partial x_i}\right)\\&+\overline{\frac{p^{'}}{\rho}\left(\frac{\partial u_i^{'}}{\partial x_j}+\frac{\partial u_j^{'}}{\partial x_i}\right)}-2\nu\overline{\frac{\partial u_i^{'}}{\partial x_k}\frac{\partial u_j^{'}}{\partial x_k}}+\nu\frac{\partial^2\overline{u_i^{'}u_j^{'}}}{\partial x_k\partial x_k}.\end{aligned} \tag{44}$$

The exact transport equations for the transport of the Reynolds stresses, R_{ij}, can be expressed as:

$$\frac{DR_{ij}}{Dt} = P_{ij} + T_{ij} + \Pi_{ij} - \epsilon_{ij} + D_{ij}, \tag{45}$$

where P_{ij} is the rate of production tensor, T_{ij} is the turbulent transport (turbulent convection) tensor, Π_{ij} is the velocity pressure gradient tensor, ϵ_{ij} is the dissipation tensor, and D_{ij} is the viscosity diffusion tensor (Bakker, 2005). Unfortunately, there is not just one equation expressing the Reynolds stresses, because these equations depend on new unknowns. The number of new unknowns increases much faster than the number of new equations derived.

From all the terms in these equations, P_{ij} is exact. It does not need any modeling. However, T_{ij}, Π_{ij}, ϵ_{ij} and D_{ij} are not exact, thus, they need to be modeled to close the equations (Bakker, 2005)(Pope, 2001).

3.2.1 The Pressure-Strain Rate Tensor

The pressure-strain rate, Ω_{ij} is the most important term to be modeled (George, 2013). It is modeled as a local function of R_{ij}, ϵ, and $\partial\overline{u_i}/\partial x_j$,

$$\Omega_{ij} = \overline{\frac{p^{'}}{\rho}\left(\frac{\partial u_i}{\partial x_j} + \frac{\partial u_j}{\partial x_i}\right)}. \tag{46}$$

The trace of Ω_{ij} is zero (i.e. $\Omega_{ij} = 2\overline{p^{'}\nabla \cdot \mathbf{u}/\rho = 0}$). Therefore, the term is not included in the equation for the kinetic energy (obtained by contraction by setting $i = j$). It redistributes energy between Reynolds stresses. Redistribution is an important phenomenon, it ensures that the Reynolds stresses are balanced. Production and dissipation of energy is balanced by the redistribution of the pressure strain rate tensor (Pope, 2001).

For incompressible flow, the coupling of pressure and velocity can be obtained by using the continuity equation together with the divergence of the momentum equation to get a Poisson equation for pressure. By applying Reynolds decomposition to that equation, the Poisson equation for pressure is obtained:

$$\frac{1}{\rho}\nabla^2 p^{'} = -2\frac{\partial\overline{u_i}}{\partial x_j}\frac{\partial u_j^{'}}{\partial x_i} - \frac{\partial^2}{\partial x_i \partial x_j}\left(u_i^{'}u_j^{'} - \overline{u_i^{'}u_j^{'}}\right). \tag{47}$$

The fluctuating pressure can be decomposed into three parts:

$$p^{'} = p^{(r)} + p^{(s)} + p^{(h)}. \tag{48}$$

The rapid pressure $p^{(r)}$ satisfies:

$$\frac{1}{\rho}\nabla^2 p^{(r)} = -2\frac{\partial\overline{u_i}}{\partial x_j}\frac{\partial u_j^{'}}{\partial x_i}. \tag{49}$$

The slow pressure $p^{(s)}$ satisfies:

$$\frac{1}{\rho}\nabla^2 p^{(s)} = -\frac{\partial^2}{\partial x_i \partial x_j}\left(u_i^{'}u_j^{'} - \overline{u_i^{'}u_j^{'}}\right), \tag{50}$$

and the harmonic pressure p^h satisfies the Laplace equation $\nabla^2 p^{(h)} = 0$. Boundary conditions for $p^{(h)}$ defined according to $p^{(r)}$ and $p^{(s)}$, such that $p^{'}$ satisfies the required boundary conditions. The pressure strain tensor can also be decomposed into $\Omega_{ij}^{(r)}$, $\Omega_{ij}^{(s)}$, and $\Omega_{ij}^{(h)}$. The basic model for Ω_{ij} (LRR-IP):

$$\Omega_{ij} = -C_R \frac{\epsilon}{k} \left(\overline{u_i^{'} u_j^{'}} - \frac{2}{3} k \delta_{ij} \right) - C_2 \left(P_{ij} - \frac{2}{3} P \delta_{ij} \right). \tag{51}$$

The rapid pressure strain tensor contributes to the mean velocity gradients. In homogeneous turbulent flow, the rapid pressure is proportional to $\partial \overline{u_k} / \partial x_l$. The slow pressure strain rate tensor is significant in most of the cases except rapid distortion. The harmonic component is important only close to the wall; it is zero in homogeneous turbulence (Pope, 2001). It redistributes the normal stresses close to the wall (perpendicular to the wall), and increases the parallel stresses to the wall.

3.2.2 Reynolds Stress Transport

The turbulent transport (convection) term can be modeled together with the transport part of the velocity-pressure gradient by using the gradient-diffusion model: $T_{ijk} = T_{ijk}^{(u^{'})} + T_{ijk}^{(p^{'})}$.

$$T_{ijk}^{(u^{'})} = -\frac{\partial}{\partial x_k} \overline{u_i^{'} u_j^{'} u_k^{'}}, \tag{52}$$

$$T_{ijk}^{(p^{'})} = -\frac{1}{\rho} \left(\frac{\partial \overline{p^{'} u_i}}{\partial x_j} + \frac{\partial \overline{p^{'} u_j}}{\partial x_i} \right), \tag{53}$$

$$T_{ijk} = C_s \frac{\partial}{\partial x_k} \left(\frac{k^2}{\epsilon} \frac{\partial \overline{u_i^{'} u_j^{'}}}{\partial x_k} \right). \tag{54}$$

where C_s is a constant for the model. There is a more general model, which includes an anisotropic diffusion coefficient by using the Reynolds stress tensor:

$$T_{ijk} = C_s \frac{\partial}{\partial x_k} \left(\frac{k}{\epsilon} \overline{u_k^{'} u_l^{'}} \frac{\partial \overline{u_i^{'} u_j^{'}}}{\partial x_l} \right). \tag{55}$$

where $C_s = 0.22$. In order to model only $T_{ijk}^{(u^{'})}$, another model is needed which is symmetric with respect to all three indices.

3.2.3 Viscosity Diffusion Tensor

The viscosity diffusion (negligible except in near-wall region), D_{ij} can be modeled as follows by using a scalar turbulent diffusivity in order to prevent numerical instabilities:

$$D_{ij} = \frac{\partial}{\partial x_k} \left(\frac{\mu_T}{\sigma_k} \frac{\partial \overline{u_i^{'} u_j^{'}}}{\partial x_k} \right), \tag{56}$$

where the constant $\sigma_k = 0.82$ (the value for σ_k is different than the one in $k-\epsilon$ model), and $\mu_T = \rho C_\mu^{'}(\overline{\nu^2}k)/\epsilon$.

For high Reynolds number flows, the dissipation can be modeled as follows (as a result of local isotropy):

$$\epsilon_{ij} = \frac{2}{3}\epsilon\delta_{ij}. \tag{57}$$

This model is not very accurate for moderate Reynolds number flows. Moreover, the dissipation is anisotropic close to walls. Thus, in that case another model will be needed. In RSM, terms are usually modeled independent of Reynolds number except for near-wall treatments (Pope, 2001). In general, the dissipation can be modeled as follows:

$$\frac{D\epsilon}{Dt} = \frac{\partial}{\partial x_i}\left(C_\epsilon \frac{k}{\epsilon}\overline{u_i^{'}u_j^{'}}\frac{\partial \epsilon}{\partial x_j} + C_{\epsilon 1}\frac{P\epsilon}{k} - C_{\epsilon 2}\frac{\epsilon^2}{k}\right), \tag{58}$$

where $C_\epsilon = 0.15$, $C_{\epsilon 1} = 1.44$, and $C_{\epsilon 2} = 1.92$. There are two main differences in this model compared to the $k-\epsilon$ model: the production term P is calculated directly from the Reynolds stress equations, and the diffusion term has an anisotropic part.

The turbulence kinetic energy can be modeled by taking the trace (contraction of the transport equation by setting $i = j$) of the Reynolds stress tensor:

$$k = \frac{1}{2}\overline{u_i^{'}u_i^{'}}. \tag{59}$$

3.2.4 Comparison of $k-\epsilon$ Model and Reynolds Stress Model

In RSM, the turbulent-viscosity hypothesis is not used. Hence, the major problem of the $k-\epsilon$ is eliminated [6]. It is not possible to predict any RANS approach since it uses extensive modeling and has wide range of length and time scales. The $k-\epsilon$ model does not give accurate results when the flow has complex strain fields or substantial body forces (McDonough, 2007). RSM can be used at that point to get more accurate results. However, the source terms in RSM are more complex than the ones in $k-\epsilon$ model. Moreover, compared to $k-\epsilon$ model, which has six independent unknowns (Reynolds stresses), RSM has relatively more unknowns (George, 2013).

- In general, RSM is more accurate,
- RSM is computationally more expensive and difficult,
- RSM underestimates long range effects in the flow,
- Many more new unknowns are produced in transport equation of Reynolds stress; 75 unknowns in total (George, 2013),
- In $k-\epsilon$ model, there are less unknowns and less equations to be solved compared to RSM,

[6] Turbulent (or eddy) viscosity hypothesis is reasonable for simple turbulent shear flows, boundary layers, channel flows, mixing layers, etc. It performs poorly for flows with large pressure gradient, strong separation, and large streamline curvature.

- $k-\epsilon$ model overestimates turbulence,
- $k-\epsilon$ model has low computational cost.

There are seven turbulence equations to be solved (for $\overline{u_i' u_j'}$ and ϵ) in the RSM instead of two (for k and ϵ) in the case of the $k-\epsilon$ model. In general, the CPU time required to simulate the problem with RSM is twice the amount required for the $k-\epsilon$ model (Pope, 2001).

3.2.5 Overview

For every independent Reynolds stress there is one transport equation. Thus, there are six partial differential equations to be solved, which is a costly procedure. In RSM, the Reynolds stresses are treated as a functional of the velocity (i.e. the stress depends on the velocity everywhere and for all past times). For a three-dimensional flow, the RSM provides seven equations, one for a turbulence length scale and six for the Reynolds stresses.

RSM can be used in the following types of flow:

- Free shear flows with strong anisotropy,
- Flows with sudden changes in the mean strain rate,
- Flows where the strain fields are complex,
- Flows with strong streamline curvature,
- Secondary flow,
- Buoyant flow.

As it was stated in the previous section, the wall treatment in turbulent flows is very important. Due to these effects of the wall, the Reynolds stress turbulence model also needs improvements Pope (2001).

3.3 Large Eddy Simulation (LES)

The turbulence model LES lies in between RANS and DNS in terms of computational cost. DNS consumes too much resources while resolving the dissipative range, where most of the energy and anisotropy is contained in the large scales. RANS methods model all the turbulence spectrum, and results are in agreement with experiments at very high Reynolds number. However, due to extensive modeling in RANS, the results cannot be predicted. The RSM has a very large computational cost, and is not very widely used compared to $k-\epsilon$ model. The ϵ equation modeling poses the same problems as in the $k-\epsilon$ model in some types of problems, and it is unable to predict the effect of irrotational strains and not good at predicting normal stress due to being isotropic (McDonough, 2007). Thus, another method called LES is used to resolve the large scale three dimensional unsteady turbulent motions of the flow explicitly while the interactions in the small scales (dissipative range) are modeled.

Large Scales	**Small Scales**
Produced by mean flow	Produced by large scales
Inhomogeneous, anisotropic	Homogeneous, isotropic
High energy, long life	Low energy, short life
Diffusive	Dissipative
→ Difficult to model: Universal model not possible	→ Simple to model: Universal model may work

In general LES can be divided into four parts:

1. Filtering operation: Decompose velocity field in large (resolved) and small scale (SGS:= sub-grid scale); $U(x,t) = \overline{U}(x,t) + u^{'}(x,t)$, $\overline{U}(x,t)$, which is three dimensional and time dependent, represents the large eddies,
2. The filtered velocity is described by Navier-Stokes equations and SGS stress tensor,
3. Closure is provided by using the SGS stress tensor model (eddy viscosity model),
4. The filtered equations are solved for the velocity and pressure fields.

The grid size in LES is usually smaller than RANS in order to capture the small scale. For RANS models, results do not depend on grid sizes (i.e. when the desirable mesh size is achieved, finer mesh does not give better result). However, in LES models, results have grid dependency, the smaller the sizes of the grids the better the accuracy of the result. When the mesh is very fine, the result can converge to the result of DNS, in which all the flow is resolved instead of modeled.

3.3.1 Filtering

Separation of small and large scales is carried out by applying low pass filtering. Afterwards, the filtered velocity field can be resolved on a relatively coarse grid, where the necessary grid spacing Δx is defined proportional to the filter width Δ (e.g. $\Delta x = 0.5\Delta$ in contrast to $\Delta x = 2\eta$ in DNS, where η is the Kolmogorov length scale). The ideal situation for Δ can be shown to be $\Delta < l_{EI}$, where l_{EI} is the size of the smallest energy motions.

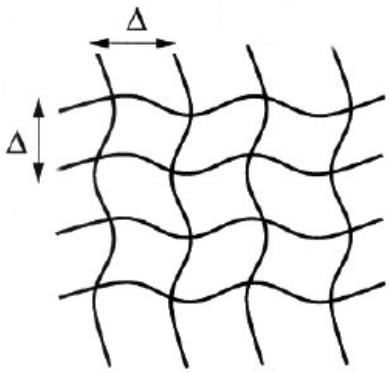

Figure 5: Filter

Large eddies (coarse structures) are bigger than Δ, however, small eddies (fine structures) are smaller than Δ.

At a given point x in the computational domain, the filtering operation is expressed as:

$$\overline{U}(x,t) = \int G(r,x)U(x-r,t)dr. \tag{60}$$

where G is the specified filter function, and the integral is all over the entire flow domain. The filter function satisfies

$$\int G(r,x)dr = 1. \tag{61}$$

The simplest filter is the homogeneous filter: $G(r,x) = G(r)$ (at every point the same filter is applied). Gaussian, box, and spectral filters are the the most commonly used filters (Avila, 2015).

The residual velocity field is defined by

$$u^{'}(x,t) = U(x,t) - \overline{U}(x,t). \tag{62}$$

Thus, the velocity field is decomposed similarly as the Reynolds decomposition;

$$U(x,t) = \overline{U}(x,t) + u^{'}(x,t). \tag{63}$$

$u^{'}(x,t)$ is time dependent. Hence the filtered residual is not zero: $u^{'}(x,t) \neq 0$.

The filtered velocity can be expressed by a convolution in one dimension

$$\overline{U}(x) = \int_{-\infty}^{\infty} G(r)U(x-r)dr. \tag{64}$$

Conservation equations need to be formulated for the filtered velocity field (homogeneous filter, $G(r)$ is considered). In order to obtain the equations, the filtering operation is applied to the Navier-Stokes equations. The filtered continuity equation is

$$\left(\overline{\frac{\partial U_i}{\partial x_i}}\right) = \frac{\partial \overline{U}_i}{\partial x_i} = 0. \tag{65}$$

Thereby, under the assumption that filtering and differentiation commute, gradient of the residual velocity field is

$$\frac{\partial u_i^{'}}{\partial x_i} = \frac{\partial}{\partial x_i}(U_i - \overline{U}_i) = 0. \tag{66}$$

For the momentum equation the filtering operation results in the following equation:

$$\frac{\partial \overline{U}_j}{\partial t} + \frac{\partial \overline{U_i U_j}}{\partial x_i} = \nu \frac{\partial^2 \overline{U}_j}{\partial x_i \partial x_i} - \frac{1}{\rho}\frac{\partial \overline{p}}{\partial x_j}, \tag{67}$$

where $\overline{p}(x,t)$ is the filtered pressure field. The residual stress tensor is introduced in order to make this equation similar to the Navier-Stokes equation ($\overline{U_i U_i} \neq \overline{u}_i \overline{u}_j$):

$$\tau_{ij}^R = \overline{U_i U_j} - \overline{U}_i \, \overline{U}_j, \tag{68}$$

$$\overline{U_i U_j} = \tau_{ij}^R + \overline{U}_i \, \overline{U}_j. \tag{69}$$

The residual kinetic energy is

$$k_r = \frac{1}{2}\tau_{ij}^R, \tag{70}$$

and the anisotropic residual stress tensor is defined as

$$\tau_{ij}^r = \tau_{ij}^R - \frac{2}{3}k_r\delta_{ij}. \tag{71}$$

When the filtered pressure is expressed as $\overline{p} = \overline{p} + 2/3\rho k_r$, the isotropic part of the residual stress is obtained. The modified filtered momentum equation is

$$\frac{\partial \overline{U}_j}{\partial t} + \overline{U}_i\frac{\partial \overline{U}_j}{\partial x_i} = \nu\frac{\partial^2 \overline{U}_j}{\partial x_i \partial x_i} - \frac{\partial \tau_{ij}^r}{\partial x_i} - \frac{1}{\rho}\frac{\partial \overline{p}}{\partial x_j}. \tag{72}$$

The filtered Eq. (72) is not closed as it was the case in $k-\epsilon$ model and RSM. Thus, the equation should be closed by modeling the residual stress tensor τ_{ij}^r. The residual stress tensor introduces additional dissipation: It removes energy from large scales and the energy is transferred to the smaller scales. The filtered velocity $\overline{U}_i$ depends on the filter (type, width) indirectly through the model for τ_{ij}^r.

The convective flux is defined as

$$\overline{U_i U_j} := \overline{U_i}\,\overline{U_j} + \tau_{ij}^R = \overline{U_i}\,\overline{U_j} + \tau_{ij}^r + \frac{2}{3}k^r\delta_{ij}, \tag{73}$$

where the decomposition of the residual stress is

$$\tau_{ij}^R := L_{ij} + C_{ij} + R_{ij}, \tag{74}$$

$$L_{ij} := \overline{\overline{U_i}\,\overline{U_j}} - \overline{U_i}\,\overline{U_j}, \tag{75}$$

$$C_{ij} := \overline{\overline{U_i}u_j'} + \overline{u_i'\overline{U_j}}, \tag{76}$$

$$R_{ij} := \overline{u_i'u_j'}. \tag{77}$$

The tensors L_{ij}, C_{ij}, and R_{ij} are called the Leonard stresses, the cross stresses, and the SGS Reynolds stresses, respectively (Wilcox et al., 1998).

3.3.2 The Smagorinsky Model

The anisotropic residual stress tensor can be modeled as follows in order to close the filtered equation:

$$\tau_{ij}^r = -2\nu_r\overline{\mathcal{S}}_{ij}, \tag{78}$$

where $\overline{\mathcal{S}}_{ij} := \sqrt{2\overline{S}_{ij}\,\overline{S}_{ij}}$ is the characteristic filtered rate of strain, $\nu_r = l_S^2\overline{S}_{ij}$ is the eddy viscosity of the residual motions, and $\overline{S}_{ij} := \frac{1}{2}\left(\frac{\partial \overline{U}_i}{\partial x_j} + \frac{\partial \overline{U}_j}{\partial x_i}\right)$ is the filtered rate of strain tensor.

The model for eddy viscosity can be expressed as:

$$\nu_r = l_S.l_S\overline{S}, \tag{79}$$

where l_S is the Smagorinsky length scale, which only affects the small scales and is proportional to the filter width, i.e. $l_S = C_S\Delta$, and C_S is the Smagorinsky coefficient. The second part, $l_S\overline{S}$ expresses the velocity part.

The rate of transfer of the energy to the residual motion is

$$P_r = -\tau_{ij}^r \overline{S}_{ij} = 2\nu_r \overline{S}_{ij}\overline{S}_{ij} = \nu_r \overline{S}^2 > 0, \tag{80}$$

which means energy is always removed since $\nu_r > 0$ (i.e. the energy is transferred only from filtered to the residual motion).

The mean energy transfer is balanced by the dissipation ϵ for high Reynolds number flows and a filter width in the energy containing range (production subrange) and dissipation range (viscous subrange); in the inertial subrange (i.e. $l_{EI} > \Delta > l_{DI}$):

$$\epsilon = \overline{P}_r = \overline{\nu_r \overline{S}^2} = l_S^2 \overline{\overline{S}^3}. \tag{81}$$

The LES equation itself does not depend on the chosen filter. The filter only affects $-\partial\tau_{ij}^r/\partial x_i$.

3.3.3 Wall Treatment

There are two specific approaches for wall treatment, LES with near-wall resolution (LES-NWR) and LES with near-wall modeling (LES-NWM). In LES-NWR, the flow is resolved everywhere up to 80% of the energy, also taking into account the energy in the viscous layer (the filter and the grid spacing are fine enough). However, the flow is not resolved in near-wall region in LES-NWM. Thus, 80% of the energy is not obtained in the viscous layer.

The viscous layer is the region, where the production, dissipation, kinetic energy, and Reynolds stress anisotropy reach their maximum values (at $y^+ < 20$) (Pope, 2001). The filter width should be of the same order of the viscous length scale δ in order to resolve the viscous sublayer in near-wall region with LES-NWR. Therefore, the number of grid points required increases drastically, proportional to $Re^{1.76}$ (Pope, 2001). When the flow in the near-wall region is resolved, the number of grid point increases dramatically, which makes LES-NWR inappropriate for high Reynolds number flows.

On the other hand, LES-NWM is independent of the Reynolds number since the grid spacing and the filter width are proportional to the flow length scale l. The reason for that is the modeling of the flow in near-wall region, instead of resolving it.

3.3.4 Dynamic Model

The Smagorinsky model is improved such that inhomogeneous turbulence can be modeled. Close to the wall and for laminar flow the value of $C_S = 0$. Moreover, it has a different value for different types of flows (e.g. for high Reynolds number flows $C_S \approx 0.15$). Another model is needed in order to specify a general value for C_S.

The grid filtering with homogeneous isotropic filters:

$$\overline{U}(x.t) := \int U(x-r,t)G(|r|;\overline{\Delta})dr, \tag{82}$$

where the filter width, Δ is proportional to the grid spacing h, and the equations are solved for $\overline{U}$.

The test filter $\widetilde{\Delta}$, which is usually equal to $2\overline{\Delta}$ can be expressed as:

$$\widetilde{U}(x.t) := \int U(x-r,t)G(|r|;\widetilde{\Delta})dr, \tag{83}$$

where $\widetilde{U}$ is unknown in the LES. Thus, a doubly filtered velocity field is defined as

$$\begin{aligned}\widetilde{\overline{U}}(x,t) &:= \int \overline{U}(x-r,t)G(|r|;\widetilde{\Delta})dr \\ &= \int U(x-r,t)G(|r|;\widetilde{\overline{\Delta}})dr.\end{aligned} \tag{84}$$

The effective double filter is

$$\widetilde{\overline{\Delta}} = \begin{cases} \widetilde{\Delta}, & \text{for the sharp spectral filter} \\ \left(\widetilde{\Delta}^2 + \overline{\Delta}^2\right)^{1/2}, & \text{for the Gaussian filter.} \end{cases} \tag{85}$$

By adding and subtracting the doubly filtered velocity, a decomposition of the velocity is obtained of the form

$$U = \widetilde{\overline{U}} + \left(\overline{U} - \widetilde{\overline{U}}\right) + u'. \tag{86}$$

The smallest resolved motions $\overline{U} - \widetilde{\overline{U}}$ (eddies of size between $\overline{\Delta}$ and $\widetilde{\overline{\Delta}}$) can be found by using $\overline{U}$. They are resolved by using the grid filter $\overline{\Delta}$, but they are not captured with the test filter.

Now by using Germano's Identity the residual stresses can be defined with the single and double filtering operations separately:

$$\tau_{ij}^R := \overline{U_i U_j} - \overline{U}_i \overline{U}_j \quad \text{(grid filter)}, \tag{87}$$

$$T_{ij} := \widetilde{\overline{U_i U_j}} - \widetilde{\overline{U}}_i \widetilde{\overline{U}}_j \quad \text{(double filter)}. \tag{88}$$

The terms $\overline{U_i U_j}$ and $\widetilde{\overline{U_i U_j}}$ cannot be computed from the LES model. Thus, by applying the test filter to Eq. (87) and subtracting it from the double filter residual stress Eq. (88), the resolved stress equation can be obtained, which is possible to be computed from the LES model.

$$\mathcal{L}_{ij} := T_{ij} - \widetilde{\tau_{ij}^R} = \widetilde{\overline{U}_i \overline{U}_j} - \widetilde{\overline{U}}_i \widetilde{\overline{U}}_j. \tag{89}$$

The resolved stress $\mathcal{L}_{ij}$ contributes to the residual stress from the largest unresolved motions.

The Smagorinsky model for the anisotropic part is

$$\tau_{ij}^r := \tau_{ij}^R - \frac{1}{3}\tau_{kk}^R \delta_{ij} = -2c_S \overline{\Delta}^2 \overline{\mathcal{S}}\, \overline{S}_{ij}. \tag{90}$$

By using the same model for the filter width of $\widetilde{\overline{\Delta}}$ (double filter) the following expression is obtained

$$T_{ij}^a := T_{ij} - \frac{1}{3}T_{kk}\delta_{ij} = -2c_S\widetilde{\overline{\Delta}}^2\,\widetilde{\overline{\mathcal{S}}}\,\widetilde{\overline{S}}_{ij}. \tag{91}$$

For simplification assume c_S is uniform and define $M_{ij} := 2\overline{\Delta}^2\widetilde{\overline{\mathcal{S}}\,\overline{S}}_{ij} - 2\widetilde{\overline{\Delta}}^2\,\widetilde{\overline{\mathcal{S}}}\,\widetilde{\overline{S}}_{ij}$. Then the Smagorinsky model of the anisotropic part of the resolved stress is:

$$\mathcal{L}_{ij}^S := T_{ij}^a - \widetilde{\tau_{ij}^r} = c_S M_{ij}, \tag{92}$$

where the anisotropic part of $\mathcal{L}_{ij}$ is

$$\mathcal{L}_{ij}^a := \mathcal{L}_{ij} - \frac{1}{3}\mathcal{L}_{kk}\delta_{ij}. \tag{93}$$

Now, the optimal value for c_S should be selected, which provides the best approximation. It is important to note that $\mathcal{L}_{ij}^a$ and $\mathcal{L}_{ij}^S$ have five independent components. Therefore, mean-square error minimization is used in order to find a suitable c_S value that satisfies all the components:

$$c_S = \frac{M_{ij}\mathcal{L}_{ij}}{M_{kl}M_{kl}}. \tag{94}$$

In channel flow, the value of c_S that is obtained by using Eq. (94) leads to fluctuations because of the low correlation between the rate of strain and the stress. Therefore, another method can be used to obtain stable results for LES. With this method, the value for c_S is obtained by taking averages:

$$c_S = \frac{(M_{ij}\mathcal{L}_{ij})_{avg}}{(M_{kl}M_{kl})_{avg}}, \tag{95}$$

and this method yields good results for transitional and fully turbulent channel flow (Pope, 2001). It also provides the right value at the wall and for the laminar flow. Moreover, there is no need for additional wall treatment if the grid is fine enough to resolve the near-wall region.

3.3.5 Overview

The smallest finite difference cells in LES can be larger than the Kolmogorov length scale. Therefore, larger time steps can be taken compared to DNS. This leads to less computational effort (in terms of memory and CPU) than DNS since it models the smallest eddies. The number of grid nodes required for a channel flow with LES, N_{LES} is calculated by using Eq. (2).

In order to decrease the total time to solve the problem with LES, wall functions can be imposed as a boundary condition, which will reduce the resolution requirements. If the law of the wall is used in the viscous sublayer, then the number of grid points decreases. However, using the law of the wall as a boundary condition cannot predict fluctuating values in the log-law region. Thus, the law of the wall may not be sufficient to see the changes of the kinetic energy and dissipation in LES (Wilcox et al., 1998). On the other hand, it is expensive to resolve the the near-wall region at high Reynolds number flows.

Wall stress models can be used to provide necessary wall stresses to the LES. In this way, computational cost will significantly decrease with the usage of the model.

For free shear flows, although the small-scale turbulence in the initial part of the shear layer is not adequately resolved, LES is still a good choice since the computational cost of LES is independent of the Reynolds number. For pipe flows, LES is not quite practicable since the motions that contain energy near the wall are hard to resolve. However, for this difficulty one can use LES-NWM to model the near-wall region and decrease the cost of the problem.

An important difference between LES and RANS is that LES is time dependent, whereas RANS is time averaged. The main differences between the Reynolds stress equations and filtered equations are the field ($\overline{U}_i, \overline{p}$, and τ_{ij}^r) properties, which are random, three dimensional, and time dependent. The transition from laminar to turbulent flow can be captured with LES.

The computational time of incompressible fully developed smooth pipe flow at $Re = 100,000$ for LES is between 400-480 hours, for $k-\epsilon$ model it is between 55-60 hours, and for Reynolds stress model it is between 80-100 hours (Vijiapurapu and Cui, 2010).

3.4 Estimating Problem Complexity for Different Turbulence Models

Modeling of multiphase turbulent flows with high accuracy is more difficult modeling single-phase turbulent flows. Although, the interface between two immiscible phases can be described quite precisely with available models, the influence of the turbulent fluctuations in one of the phases may have great influence on the dynamics of the interface. Therefore, it is very important to clarify the effect of the turbulence in all phases.

With an increase in the air velocity, the interface becomes oscillatory without showing regular wave patterns. This is caused by the turbulence in the gas phase. Around a gas velocity of 3.5 m/s waves start to appear on the interface. The transition from smooth interface to wavy interface also depends on the velocity of the liquid phase.

There are some studies about turbulent two-phase stratified pipe flow but not much of them have been carried out with LES since it is not a common practice in turbulent two-phase stratified pipe flow. Therefore, in order to have an idea about the flow properties, first, DNS and LES are used for single-phase turbulent pipe flow, then, necessary inferences are made about turbulent two-phase pipe flow. However, an estimation approach for the RANS equations are not considered since the limitations (which are almost negligible) imposed by RANS are quite less than the limitations imposed by DNS and LES. Also, the Reynolds number is too low for doing RANS. By estimating the number of total grid points required for single-phase turbulent flow, a minimum requirement and an insight about the complexity of turbulent two-phase flow is obtained.

3.4.1 Computational Costs

The experiments that have been carried out by Birvalski (2015) are used for validation. In these experiments, the diameter of the pipe is $D = 50\ mm$, and the length of the pipe

is $L = 200D = 10\ m$. The superficial water flow rates are 0.0085 m/s and 0.0255 m/s, and the superficial air velocity varies from 0 to 5.4 m/s (non-wavy surface between 0 and 1 m/s) to obtain both laminar and turbulent flow respectively.

As the velocity of the air varies in the experiments, the velocity of the liquid also varies due to the momentum transfer between the phases at the interface. When the air velocity is $u_G = 1.04\ m/s$, the gas phase is turbulent, and the liquid in the two-phase flow also becomes (stratified) turbulent at a liquid velocity $u_L = 0.1126\ m/s$ with an intermittency factor 0.99 and a Reynolds number $Re_L = u_L D/\nu = 3421$. The Reynolds number for the air at that velocity is $Re_G = 3632$ (Birvalski, 2015).

The length of the problem domain that is resolved should be long enough to accommodate the largest turbulence structures. In channel flow, eddies are stretched parallel to the channel walls, and their length is approximately equal to $2H$, where H is the height of the channel (Wilcox et al., 1998). For pipe flow, in order to compute the required pipe length for an accurate model that includes the largest turbulent structures, the two-point correlation coefficient of the velocity fluctuations in the streamwise direction can be calculated. According to the result in the work of Eggels (1994), the required pipe length to resolve the larges scale structures for the given Reynolds number should be $L_x = 2.5D = 125\ mm$, where L_x is the required length in parallel wall direction, namely x.

First, the approach is directed towards LES of channel flow in this thesis to get an initial insight for the pipe flow. The required number of grid points in turbulent channel flow can be estimated for DNS with the equation below

$$N_L = \frac{L}{\Delta x} \sim \frac{10l}{\eta} = 10Re_l^{3/4}, \tag{96}$$

where Δx is the grid spacing, length scales L represents the flow geometry (e.g., the pipe diameter), η is the Kolmogorov length scale (smallest eddies), l $[m]$ represents the largest eddies in the flow, and $Re_l \approx Re_L/170 \approx 3421/170 \approx 20$ for water and $Re_l \approx Re_G/170 \approx 3632/170 \approx 21$ for air [7]. Thus, the total number of grid points for water in three dimensions N_L^3 is proportional to

$$N_L^3 \sim 10Re_l^{9/4} \sim 10(20)^{9/4} \sim 8.5 \times 10^3, \tag{97}$$

and for air

$$N_L^3 \sim 10Re_l^{9/4} \sim 10(21)^{9/4} \sim 9.5 \times 10^3. \tag{98}$$

According to the studies, at $Re_L = 3421$ the LES can be resolved near-wall region since the CPU time does not differ significantly compared to the modeled near-wall region case (Gnambode et al., 2015). The number of grid points is proportional to

$$N_L = \frac{L}{\Delta x} = \frac{L}{l}\frac{l}{\Delta}\frac{\Delta}{\Delta x} \approx 20\frac{l}{\Delta}. \tag{99}$$

where the ratio of the flow geometry to the largest length scale is approximated as $L/l \approx 10$ for wall-bounded shear-driven turbulent flows (Eggels, 1994). The filter length Δ is

[7] In general case, the Reynolds number is expressed as $Re = U_b D/\nu$ where U_b being the mean velocity, D is the pipe diameter. The Reynolds number $Re_l = ul/\nu$ can be approximated by using ($l \sim \frac{1}{10}D$) and ($u \sim \frac{1}{17}U_b$), hence, $Re_l = ul/\nu \approx Re/170$.

assumed to be double the grid spacing, i.e., $\Delta \approx 2\Delta x$, in order to keep the range of grid scale motions as large as possible.

For LES, the ratio of l/Δ plays an important role in computations (instead of Re_l as it is the case for DNS). The computational cost increase rapidly as the ratio gets larger. Furthermore, LES computations give realistic results when the ratio is large (e.g., $l/\Delta > 10$). The reason behind this is the increase in the range of turbulent length scales that are resolved and the decrease in the range of length scales that are used in SGS stress tensor when the ratio increases. However, in the study of Eggels (1994), the computations of LES are considered to be realistic when the ratio is even smaller (i.e., $l/\Delta > 2$). As the ratio gets smaller, the SGS closure model becomes important, whereas the range of resolved grid scale decreases. In the study of Eggels (1994), when the value of the ratio is around 1, computations are considered to be unrealistic. The smallest value that gives realistic LES results used in their study is 1.8.

In our case, the ratio is taken as $l/\Delta = 5$, and the length scale in the radial direction for the pipe flow case L_r is equal to the pipe diameter $L_r = D = 50\ mm$ and in the streamwise direction $L_z = 2.5D = 125\ mm$. Hence, for the axial direction $l \approx 12.5\ mm$, and $\Delta = 2.5\ mm$, which results in the following number of grid points:

$$N_L \approx 20\frac{l}{\Delta} \approx 100. \tag{100}$$

DNS	Water
N_r	11
N_θ	248
N_z	198
N_{total}	5×10^5

Figure 6: Computational cost for DNS with only water

The estimation of the number of grid points for DNS is explained in Appendix A and the estimation of the number of grid points for LES is explained in Appendix B in detail for the pipe flow under consideration. The number of grid points required for DNS of single phase water flow with non-uniform grid spacing in radial direction is $N_r = 11$, and with uniform grid spacing for spanwise and streamwise directions $N_\theta = 248$, $N_z = 198$ respectively. The total number of grid cells required for DNS for the liquid phase are approximately 5×10^5 (see Fig. 6). For the air case, the number of grid points are quite similar because of the small difference in the Reynolds numbers of liquid and gas phases.

For a well-resolved LES (resolved viscous sublayer), the near-wall grid resolution should be fine enough. The first grid-point should locate in the viscous sublayer for LES-NWR, i.e., $y^+ = 1$. The computation of the first LES case is done with grid points that are equally spaced, and the viscous sublayer is not resolved, i.e., the first grid-point is within the inertial sublayer ($y^+ = 32.8 > 30$). This approach does not need any additional damping since the first grid-point is far away from the pipe flow. The total number of grid points

is quite small for water and air phases. The reason for this is that the boundary layer is almost fully modeled because of the large value of wall unit, $y^+ = 32.8$.

For the second case, the grid spacing is non-uniform only in the radial direction (normal to the wall) and three grid points are within the viscous sublayer. The aspect ratio used in the work of Eggels (1994) is first calculated and validated in Appendix B, then used in the non-uniform case for $y^+ = 1.5$.

3.4.2 Estimated Reynolds Number for the Available Computational Power

With the computational resources available in the Scientific Computing group of the Delft Institute for Applied Mathematics, which corresponds to $30 \times 150 \times 90$ grid points, the problem can be modeled both with DNS and LES for the given Reynolds numbers with serial algorithms in a reasonable amount of time. However, the estimations show that LES is quite less demanding than DNS since the Reynolds number is relatively smaller for doing LES. Therefore, LES can be considered to be feasible for both water and air flows considering the computational cost especially when the computational domain length is larger.

The maximum computational capacity is slightly exceeded with DNS. On the other hand, the maximum possible value of the Reynolds number for LES can be approximated with the available computational power (i.e., $4{\times}10^5$ is the maximum number for total grid points).

For LES with non-uniform grid spacing, the Reynolds number that was used for the calculations is not large enough to exceed the computational limitations. When the Reynolds number is approximately equal to 4×10^4, then the required number of grid points in r-direction is $N_r \approx 33$. The dimensionless mesh width in r-direction for the calculated number of grid points is approximately equal to 0.0166. The approach implemented in the Appendix B is applied here and the required mesh width in θ- and z- direction can be calculated as 0.26166 and 0.02768 respectively. For these uniform grid spacings, the required number of grid points are 120 and 90 respectively for θ- and z-direction. The available computational power is almost fully used with these number of grid points that are obtained for the chosen Reynolds number value of 4×10^4.

4 The Physics and Model of Stratified Two-Phase Flow

Turbulence in two-phase flow may be very different from single phase flow. In single phase turbulent flow, one needs to model the Reynolds stress terms to obtain the closure relations. However, in two-phase flow many more closure relations are needed. Unlike single phase flow, there is no universal model that describes the instability that causes the transition to another flow pattern in two-phase flow.

In the presence of waves, the turbulence behaves differently compared to the turbulence in shear layers. At the interface, the fluctuations occur mostly because of the effect of the wave motion. In two-phase flow, there are two main reasons for the formation of fluctuations. One of them is the turbulence created by shear stresses in near-wall region, and the other one is induced by wave motions.

It is known that the turbulence due to shear in the wave region behaves similarly as the turbulence in single-phase flow. Moreover, the physics of momentum transfer at the waves can be identified more precisely with LES since mass, momentum, and energy transfers occur at the interface (where the flow is resolved for large scales in LES). Therefore, LES seems to be the promising method.

4.1 Dimensionless Parameters

The finite thickness layer, where the material properties change, between two phases is called the *interface*. Surface tension occurs at the interface due to the attractive forces acting on molecules. In two-phase flows, the change in viscosity due to different material properties and the existence of surface tension forces at the interface lead to jumps and discontinuities at the interface for pressure and the gradient of the velocity field.

In order to identify the dominant forces acting on the flow, these forces should be compared using dimensionless groups. This way some forces may be neglected and the problem becomes easier to handle. Dimensionless variables are defined by a characteristic length L, a velocity scale U, and a time scale τ;

$$x = Lx^*, \quad u = Uu^*, \quad t = \tau t^*. \tag{101}$$

where x^*, t^*, and u^* are the dimensionless variables. The *Strouhal number Sl* is defined by

$$Sl = \frac{U\tau}{L}. \tag{102}$$

It can be interpreted as the ratio of the time scale τ to the convective time scale L/U. The *Reynolds number Re*, which describes the ratio of inertial forces to the viscous forces, is defined by

$$Re = \frac{\rho LU}{\mu} = \frac{LU}{\nu}. \tag{103}$$

The *Euler number Eu*, which represents the ratio of pressure gradient to inertia forces, is defined by

$$Eu = \frac{\Delta p}{\rho U^2}. \tag{104}$$

The *Froude number Fr* characterizes the ratio of inertia and gravity forces and it is defined by

$$Fr = \frac{U^2}{gL}, \tag{105}$$

where g is the gravitational force acting on the flow, it can also be another type of force. For the surface tension force, the *Weber number We*, which expresses the ratio of inertial forces to surface tension forces (i.e. curvature), is used:

$$We = \frac{\rho L U^2}{\gamma}. \tag{106}$$

The *Eötvös number Eo* or *Bond number* is the ratio of gravity to surface tension forces (capillary force scales):

$$Eo = \frac{|\rho - \rho^{'}|gL^2}{\gamma}, \tag{107}$$

where $\rho^{'}$ is the density of the gas bubbles. The *Capillary number Ca*, which represents the ratio of viscous forces to surface tension forces, is equal to:

$$Ca = \frac{We}{Re} = \frac{\mu U}{\gamma}. \tag{108}$$

The *Morton number Mo* is defined as:

$$Mo = \frac{g\mu^4}{\rho\gamma^3}. \tag{109}$$

Not all of these dimensionless parameters are relevant for this problem. For example, the Strouhal number is commonly used in fields such as bluff body flows. However, the Reynolds number, which represents the flow pattern (i.e. laminar or turbulent), is certainly an important parameter for this project. The Euler number, which is not very relevant for this problem, is used to describe the losses in the flow. The Froude number represents the behavior of surface waves and flow interactions at a cross section. Thus, it is a relevant dimensionless parameter for this study. The Weber number is used to analyze the formation of droplets and bubbles. It can be used in this study since the influence of the pipe diameter on the flow regimes can be expressed with this dimensionless parameter. The Eötvös number, which is needed when there are large gas bubbles, is used to analyze the surface tension in the two-phase microchannel flows. The Capillary number, which is commonly used in flows with liquid drops or plugs, is also not relevant to this study since the viscous forces are dominant. The Morton number characterizes the shape of bubbles or drops in a flow, thus, it is not a relevant dimensionless number.

4.2 Governing Equations and Boundary Conditions at the Interface

In order to observe the influence of the interface, two phases 1 and 2 are compared at the boundary S, which separates them. When there occurs a phase change at the interface, there will be a mass flux $\dot{m}$ through the boundary. Conservation of mass gives

$$\dot{m} \equiv \rho_1 \left(\boldsymbol{u_1} - \boldsymbol{w}\right) \cdot \boldsymbol{n} = \rho_2 \left(\boldsymbol{u_2} - \boldsymbol{w}\right) \cdot \boldsymbol{n}, \tag{110}$$

where $\mathbf{n}$ is the unit normal and $\boldsymbol{w}.\mathbf{n}$ is the normal velocity of the interface. At first, if the interface is defined as

$$S(x,t) = 0, \tag{111}$$

after time dt, the surface can be expressed by taking derivative of Eq. (111),

$$\frac{\partial S}{\partial t} + \boldsymbol{w} \cdot \nabla S = 0 \quad . \tag{112}$$

By defining the unit normal as

$$\boldsymbol{n} = \frac{\nabla S}{|\nabla S|}, \tag{113}$$

the expression for $\boldsymbol{w} \cdot \boldsymbol{n}$ is obtained:

$$\boldsymbol{n} \cdot \boldsymbol{w} = -\frac{1}{|\nabla S|}\frac{\partial S}{\partial t}. \tag{114}$$

The physical parameters vary through the interface. The thickness of the interface that separates the bulk parts of two fluids is much smaller than other length scales. Thus, it is reasonable to use functional interface, in which there are two boundary conditions for the interface; *kinematic boundary condition* and *dynamic boundary condition* (Wörner, 2003). If there is no mass transfer, then at $S = 0$ the surface is impermeable $\dot{m} = 0$, thus, $\boldsymbol{n} \cdot \boldsymbol{u} = \boldsymbol{n} \cdot \boldsymbol{w}$. The equation for the kinematic boundary condition Eq. (114) is modified as:

$$\frac{\partial S}{\partial t} + \boldsymbol{u} \cdot \nabla S = 0, \tag{115}$$

and it is called the *kinematic boundary condition*. The tangential velocities at the interface for both fluids should be in balance:

$$\boldsymbol{n} \ \times \ (\boldsymbol{u} - \boldsymbol{w}) = 0. \tag{116}$$

By using Eqs. (112) and (116), it can be shown that:

$$\boldsymbol{u} = \boldsymbol{w}. \tag{117}$$

For steady state flow, the kinematic boundary condition can be expressed as:

$$\boldsymbol{u} \cdot \boldsymbol{n} = 0. \tag{118}$$

Another condition for the interface is that the momentum (the pressure and viscous stresses) is balanced through the interface by the force acting due to surface tension. When two fluids are viscous, the tangential velocity across the interface is continuous (when $\dot{m} = 0$):

$$\boldsymbol{u_1} = \boldsymbol{u_2}. \tag{119}$$

This is called the *dynamic boundary condition*:

$$\boldsymbol{n} \cdot T_1 - \boldsymbol{n} \cdot T_2 = \sigma \boldsymbol{n} \left(\nabla_s \cdot \boldsymbol{n}\right) - \nabla_s \sigma, \tag{120}$$

where $\boldsymbol{T} = \boldsymbol{\tau} - \boldsymbol{p}\mathrm{Id} = \mu\left(\nabla \boldsymbol{u} + \nabla \boldsymbol{u}^{\boldsymbol{T}}\right) - \boldsymbol{p}\mathrm{Id}$ is the stress tensor, Id is the identity tensor, $\nabla_s = (\mathrm{Id} - \boldsymbol{n_1 n_1}) \cdot \nabla$ is the surface gradient operator and σ is the surface tension. When there is no shear stress, the expression for static interfaces is (Young-Laplace)

$$p_1 - p_2 = \sigma \mathcal{K} = \sigma \left(\frac{1}{R_1} + \frac{1}{R_2}\right). \tag{121}$$

where $\mathcal{K} = \nabla_s \cdot \boldsymbol{n} = \left(\frac{1}{R_1} + \frac{1}{R_2}\right)$ is the mean curvature of the interface. Normal stress balance is

$$\boldsymbol{n} \cdot T_1 \cdot \boldsymbol{n} - \boldsymbol{n} \cdot T_2 \cdot \boldsymbol{n} = \sigma \left(\nabla_s \cdot \boldsymbol{n}\right). \tag{122}$$

The tangential stress balance with tangential unit vector $\boldsymbol{t}$ is

$$\boldsymbol{n} \cdot T_1 \cdot \boldsymbol{t} - \boldsymbol{n} \cdot T_2 \cdot \boldsymbol{t} = -\nabla\sigma \cdot \boldsymbol{t}. \tag{123}$$

4.3 Overview of the Governing Equations

The two phases are considered Newtonian, immiscible and incompressible. The phase with the higher density flows on the bottom of the pipe. The governing equations for the two-phase stratified flow are Navier-Stokes equations in both domains Ω_α and Ω_γ (see Fig. 7). The continuity equation for a phase with density ρ_α is

$$\nabla \cdot \boldsymbol{u_\alpha} = 0. \tag{124}$$

The conservation equation for momentum is

$$\rho_\alpha \frac{\partial \boldsymbol{u_\alpha}}{\partial t} + \rho_\alpha \nabla \cdot (\boldsymbol{u_\alpha u_\alpha}) = -\nabla p_\alpha + \nabla \cdot \tau_\alpha + \boldsymbol{F_\alpha}, \tag{125}$$

where τ_α is the deviatoric stress tensor and $\boldsymbol{F_\alpha}$ represents the force per unit volume acting on the phase α.

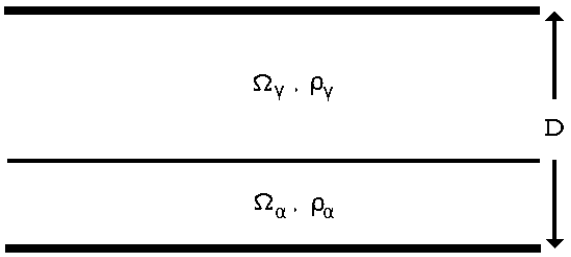

Figure 7: Schematic representation of stratified pipe flow.

Eqs. (124) and (125) for phase α are subject to the following boundary conditions (at the interface S between phase α and γ, see Fig. 8) are

$$\rho_\alpha(\boldsymbol{u}_\alpha - w) \cdot \boldsymbol{n}_\alpha + \rho_\gamma(\boldsymbol{u}_\gamma - w) \cdot \boldsymbol{n}_\gamma = 0, \tag{126}$$

$$\rho_\alpha \boldsymbol{u}_\alpha(\boldsymbol{u}_\alpha - w) \cdot \boldsymbol{n}_\alpha + \rho_\gamma \boldsymbol{u}_\gamma(\boldsymbol{u}_\gamma - w) \cdot \boldsymbol{n}_\gamma = \tag{127}$$

$$(-p_\alpha \mathrm{Id} + \tau_\alpha) \cdot \boldsymbol{n}_\alpha + (-p_\gamma \mathrm{Id} + \tau_\gamma) \cdot \boldsymbol{n}_\gamma - \nabla_S \sigma_{\alpha\gamma} + \frac{2\sigma_{\alpha\gamma}}{|\nabla S|} \nabla S.$$

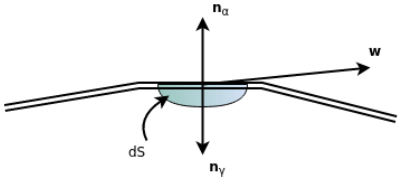

Figure 8: A fraction of the interface between phases α and γ.

5 Turbulence Modeling for Two-Phase Turbulent Flow

5.1 Literature Review

DNS and LES give more accurate results at low Reynolds number. The computational effort required for DNS is not significantly more than LES for low Reynolds number (i.e., $Re \approx 3000$). It was realized during the estimation procedure that modeling the problem with DNS is realistic even for the two-phase case. However, unlike LES, DNS is not feasible for a higher Reynolds number flow. Therefore, LES of two-phase turbulent flow is the major focus of this thesis in order to predict onset of instability of the interface and the formation of slug.

Most of the DNS and LES studies in the literature are carried for channel flows. Nevertheless, there are few studies about LES of pipe flows. However, simulation of the turbulent two-phase stratified pipe flow is even more sparse, and LES is not a widely used turbulence model for this case.

The earliest study of LES for single phase pipe flow is the work of Eggels et al. (1994). Eggels (1994) also performed LES computations for single phase pipe flows, and the results of DNS and LES were compared with experimental results. Eggels and Nieuwstadt (1993) used LES for rotating turbulent single phase pipe flow, and LES of turbulent curved single phase pipe flow was carried out by Boersma and Nieuwstadt (1996). LES study for turbulent two-phase stratified pipe flow is very limited. Therefore, initially in this thesis, LES studies that are not necessarily for pipe flow and do not include momentum transfer between two different phases are considered. In addition to this, studies about other turbulence models are also compared since LES is not the common method for modeling turbulent two-phase stratified pipe flow.

In the master thesis of Chinello (2015), the turbulence behavior of the interface in stratified two-phase flow has modeled with the classical $k-\omega$ low Reynolds number correction model and with the modified $k-\omega$ model in order to predict more accurately. Available works in the literature about stratified two-phase flow with RANS have analyzed and compared in this thesis. In this thesis, the flow has simulated in 1-D and a new input parameter, which represents the wavy motion at the interface, has implemented to the model to obtain results close to the experimental results. In order to realize the momentum transfer in between two phases, necessary adjustments were made to the grid and to the model. The turbulence near the gas side of the interface has assumed to be similar to the one near the wall, which was indicated by the DNS studies of Lombardi et al. (1996) and Fulgosi et al. (2003). The thesis has pointed out that there is no optimum and robust method that simulates turbulent two-phase stratified flow.

In the study of Labourasse et al. (2007), the flow in both phases and turbulence at the interface is resolved using the complete filtered two-phase flow governing equations. The mathematical formulation was based on one-fluid model, which means that the interaction between two phases needs to be modeled. The filtering and averaging operations yield terms for turbulence and interface. According to the study, LES is reasonable when the small turbulent scales are much smaller than the scale of the interface and it is very hard to analyze the behavior of the turbulence at the interface. A front-tracking method with a defined sharp interface, which does not use the usual smoothing function of the interface,

was used in the study to model the interface explicitly. Results showed that the volume filtering method overestimates the momentum transfer, mass-weighted filtering process underestimates the momentum transfer. Therefore, the work has recommended the use of a mass-weighted filtering process for modeling two-phase turbulent flow. The interfacial terms are very important for the turbulence behavior of the phases, and the interface can absorb some of the energy of the turbulence and advects it to the other phase. The study has also shown that the inertia term cannot be modeled with a viscosity assumption and it was exhibited different behavior than the single-phase flow near the interface.

Lamarque et al. (2010) modeled the turbulent free-surface flow in an unbaffled stirred tank reactor with LES. The study emphasizes the limitations of RANS methods compared to Reynolds stress models and LES (in terms of the mean flow characteristics) for the given problem, which consists of rotation of the stirrer. The stirrer was modeled by using an immersed boundary method and a front-tracking method was used to capture the free-surface vortex. In the work, most of the mean and fluctuation characteristics were successfully computed by LES.

In the study of Berthelsen and Ytrehus (2005), a modified two-layer turbulence model is used in order to account for the wavy interface, which is modeled as a rough interface, and for the turbulent viscosity in a fully developed stratified wavy two-phase flow in a pipe. The turbulence model consists of a two-equation k-ϵ model and a one-equation k-l model with an interfacial roughness has provided the results for the interfacial shear stress without the use of wall functions. In the method, the immersed interface method has been used to treat interfacial boundary conditions. A parameter, which has a small effect on the results, has been used to represent the interfacial roughness. The results have been shown to be in an agreement with experimental results.

Ghorai and Nigam (2006) stated in their study that modeling of smooth stratified flow is not a problem since the smooth friction factor can be easily expressed. However, for wavy stratified flow, there are two possible approaches to take: First one is to propose a global empirical correlation for the interfacial friction factor, and the second approach is to define the interface as an interfacial roughness by using the idea behind shear flow. The interfacial roughness has been estimated by defining a ratio between the interfacial friction factor and the wall friction factor.

In the study of Ullmann and Brauner (2006), the momentum transfer at the interface was considered to be the crucial issue in modeling of two-phase (gas-liquid) stratified flows. The main approach used in most of the studies and also in this one was to extrapolate the information gathered from the single phase flow and to obtain empirical correlations based on experimental data. According to the study, the values of the liquid wall shear and the interfacial shear was increased as waves get larger compared to the values predicted for smooth stratified flow. The results of the study shows that the interaction between the phases can be expressed with the closure relations that were used in the study.

The numerical simulation of slug flow in horizontal pipes was carried out by Frank (2003). Two-fluid approach was used in the study and it was showed that the wall friction of the liquid phase has a significant affect on the formation of slugs. The formation of slugs also depends on the perturbation in the inlet boundary condition and the length of the computational domain.

Lakehal et al. (2012) has examined the development of large-wave structures in two-phase turbulent pipe flow using the Level Set method for interface tracking and VLES (Very-Large Eddy Simulation) for turbulence modeling. The VLES used in the study is based on a $k-\epsilon$ subgrid model in order to include the effect of sub-scale turbulence. The reason for a more detailed subgrid scale turbulence model compared to a zero-equation model like in LES is to filter a larger part of turbulent fluctuations. In the study of (Lakehal et al., 2011), LES and VLES methods have been used for turbulence modeling and Level Set method has been used to model the free surface flow, for interface tracking. it has shown that the Level Set method predicts the transition of a gas-liquid stratified flow to slug flow with an accuracy that is better than the two-fluid phase-average model.

5.2 Influence of Interface on Turbulence

The increase in the velocity of the gas phase can produce waves at the interface. The wavy interface can be modeled as a solid surface with appropriate an surface roughness, in which, the liquid phase acts as a stationary wall since it has a smaller velocity than the gas phase. The velocity difference between two phases creates a shear stress, which can be called as *interfacial shear stress*.

In addition to the interfacial shear stress, the wall shear stress also needs to be calculated in order to model the momentum transfer between phases. However, the wall stress at the wall is different for both liquid and gas phases. Therefore, first, a single-phase wall shear stress is calculated by assuming only the liquid or gas phase flows in the pipe. Then, in a later stage, the two-phase wall shear stress is calculated by applying a multiplier to the single-phase shear stress. This method is called a *separated flow* model, which differs from a *homogeneous-flow* model in the sense that both phases are not assumed to flow together at the same velocity. Also, in homogeneous flow model, the two phases are assumed to flow as a single-phase with weighted averaged properties of both phases. On the other hand, the *two-fluid* model is the most complicated and detailed model, which requires information about flow properties of both phases separately, and accurate models for the transfer of mass, momentum, and energy between the phases at the interface.

The interface needs to be considered as a material surface when there are surfactants, which means it has its own density and momentum. However, in this study, the density of the interface is assumed to be zero. Hence, according to the jump conditions, mass and momentum balance at the interface (i.e., Eqs. (110) and (120)) can be applied. For the most general case, the mass transfer of the kth phase at the interface is defined by

$$\dot{m^k} = \rho^k(u^k - w) \cdot n^k. \tag{128}$$

The mass balance for all phases is

$$\sum_k \dot{m}^k = \sum_k (\rho^k(u^k - w) \cdot n^k) = 0. \tag{129}$$

The balance of momentum for the kth phase throughout the interface (i.e., Eq. (120)) yields:

$$\sum_k \Big(u^k \dot{m}^k - n^k \cdot (\tau^k - p^k \mathrm{Id}) \Big) = \sigma n^k \nabla_s \cdot n^k - \nabla_s \sigma, \tag{130}$$

where ∇_s is the surface gradient operator.

$$\tau^k = \mu^k S_D^k \tag{131}$$

is the deviatoric stress tensor, S_D^k is defined as

$$S_D^k = \left(S^k - \frac{1}{3}\mathrm{tr}(S^k)\mathrm{Id} \right), \tag{132}$$

where $S = \nabla u + \nabla^T u$ is the deformation rate tensor, and tr stands for the trace of a tensor.

In order to extend each phase to the whole domain, there is a need to define the interface of the kth phase as a function of position and time. For each phase a *phase indicator function or characteristic function* $\chi^k(\mathrm{x}, t)$ can be defined as:

$$\chi^k(x,t) = \begin{cases} 1, & \text{if x} \in \text{ the } k\text{th phase} \\ 0, & \text{if x} \notin \text{ the } k\text{th phase} \end{cases} \tag{133}$$

If the given position vector is in the interface (i.e., $\mathrm{x} \in S$), then the function $\chi^k = 0$, the other way round is also true. The function χ^k is defined such that it complies several properties. The two phase indicator functions are related:

$$\chi^1 + \chi^2 = 1. \tag{134}$$

The gradient of the phase indicator function can be expressed in terms of the Dirac delta function of the interface $\delta(\mathrm{x}-\mathrm{x}_i, t)$, where x_i is a point on the interface, and the interface unit normal vector n^k:

$$\nabla\chi^k = n^k \delta(\mathrm{x} - \mathrm{x}_i, t). \tag{135}$$

Moreover, the material derivative of χ^k is zero, which follows from the topological equation:

$$\frac{\partial \chi^k}{\partial t} + w \cdot \nabla\chi^k = 0. \tag{136}$$

The conservation of mass equation can be augmented by using a phase indicator function respectively:

$$\frac{\partial \chi^k \rho^k}{\partial t} + \nabla \cdot (\chi^k \rho^k u^k) = \rho^k (w - u^k) \cdot n^k \delta_i, \tag{137}$$

where $\delta_i = -n^k \cdot \nabla\chi^k$ is the Dirac function centered on the interface in order to describe the behavior of each phases near the interface. By applying the phase indicator function to the balance of momentum equation at the interface yields

$$\begin{aligned} \frac{\partial \chi^k \rho^k u^k}{\partial t} + \nabla\cdot(\chi^k[\rho^k u^k \otimes u^k + p^k\mathrm{Id} - \tau^k]) - \chi^k \rho^k g \\ = (\rho^k u^k \otimes (w - u^k) - p^k\mathrm{Id} + \tau^k) \cdot n^k \delta_i. \end{aligned} \tag{138}$$

The mass and momentum conservation equations defined by Eqs. (137) and (138) need to be modeled with respect to thermodynamic properties.

An approach called *one-fluid* modeling, where a single set of equations is solved for all the phases of the flow, can be used for multiphase flows by defining exactly one-fluid variable as the sum of the phase indicator weighted phases:

$$\phi = \sum_k \chi^k \phi^k. \tag{139}$$

One-fluid mass and momentum conservation equations can be written by summing all the phases of the flow. This way, the equation for the mass conservation can be simplified by using the mass jump condition, i.e., Eq. (129):

$$\frac{\partial \rho}{\partial t} + \nabla \cdot (\rho u) = 0. \tag{140}$$

The momentum conservation of the one-fluid approach is given by

$$\begin{aligned} \frac{\partial \rho u}{\partial t} + \nabla \cdot (\rho u \otimes u + p\mathrm{Id} - \tau) - \rho g \\ = \sum_k (\rho^k u^k \otimes (w - u^k) - p^k \mathrm{Id} + \tau^k) \cdot n^k \delta_i. \end{aligned} \tag{141}$$

This equation can be simplified using the jump condition for the momentum, i.e., Eq. (130):

$$\frac{\partial \rho u}{\partial t} + \nabla \cdot (\rho u \otimes u + p\mathrm{Id} - \tau) - \rho g = \nabla_s \cdot n^k \sigma n^k \delta_i - \nabla_s \sigma \delta_i. \tag{142}$$

The above mentioned one-fluid approach has been introduced by Kataoka (1986) in order to obtain results for multiphase flows by using classical single-phase flow models.

The number of unknowns of the previous equations can be reduced by using filtering or averaging methods. For this purpose, a spatial filtering operator G is defined for the LES case. As stated in Labourasse et al. (2007), the discontinuity due to the jump condition can be smoothed by using any two-phase flow numerical method (i.e., front-tracking, Level Set, and VOF) since interfaces are defined to cross computational cells in these methods. Therefore, they use filtering over the discontinuity in their work, instead of applying filtering operation over each phase separately.

The low-pass frequency filtering operator, called the volume filtering method, is defined on the computational domain $\Omega \in \mathbb{R}^3$ by

$$\overline{U}(x,t) = \int_{-\infty}^{t} \int_{\Omega} G(\overline{\Delta}(x,t), x - x^{'}, t - t^{'}) U(x^{'}, t^{'}) dx^{'} dt^{'}, \tag{143}$$

where $\overline{\Delta}$ is the cutoff length scale of the filter. The phase indicator function is filtered as

$$\alpha^k = \overline{\chi^k}. \tag{144}$$

The new term α is continuous between 0 and 1 and it is called a smooth indicator function. Moreover, the sum of α^k in every phases is equal to unity. The normal vector can be expressed in the smooth indicator function as:

$$\widehat{n^k} = \begin{cases} -\frac{\nabla \alpha^k}{\|\nabla \alpha^k\|}, & \text{if } \|\nabla \alpha^k\| \neq 0, \\ 0, & \text{otherwise.} \end{cases} \tag{145}$$

The resolved filtered Dirac function $\widehat{\delta_i}$ can be defined as

$$\widehat{\delta_i} = \|\widehat{n^k}\|. \tag{146}$$

The phase-weighted filtering of the variable ϕ^k is given as

$$\alpha^k \widetilde{\phi^k} = \overline{\chi^k \phi^k}. \tag{147}$$

By using the definitions above, the governing equations for multiphase flow can be obtained. The filtered mass conservation yields

$$\frac{\partial \alpha^k \widetilde{\rho^k}}{\partial t} + \nabla \cdot (\alpha^k \widetilde{\rho^k u^k}) = \overline{\rho^k (w - u^k) \cdot n^k \delta_i}. \tag{148}$$

The filtered momentum equation is given by

$$\begin{aligned} \frac{\partial \alpha^k \widetilde{\rho^k u^k}}{\partial t} + \nabla \cdot (\alpha^k \rho^k \widetilde{u^k \otimes u^k} + \alpha^k \widetilde{p}\mathrm{Id} - \alpha^k \widetilde{\tau^k}) - \alpha^k \widetilde{\rho^k} g \\ = \overline{(\rho^k u^k \otimes (w - u^k) - p^k \mathrm{Id} + \tau^k) \cdot n^k \delta_i}. \end{aligned} \tag{149}$$

Also, an additional equation for the evolution of the phase indicator function needs to be considered:

$$\frac{\partial \alpha^k}{\partial t} = \overline{w \cdot n^k \delta_i}. \tag{150}$$

The left-hand side of the equations represents the non-linear phase-weighted terms, and the right-hand side of the equations represents the filtered interfacial terms. In order to obtain the one-fluid model, a filtering variable $\overline{\phi}$ is defined for single fluid:

$$\overline{\phi} = \overline{\sum_k \chi^k \phi^k}. \tag{151}$$

The summation of evolution equation over all the phases together with the Eq. (151) yields the following equation for mass conservation:

$$\frac{\partial \overline{\rho u}}{\partial t} + \nabla \cdot (\overline{\rho u}) = \overline{\sum_k \rho^k (w - u^k) \cdot n^k \delta_i}. \tag{152}$$

The momentum conservation equation of the one-fluid formulation is given by

$$\begin{aligned} \frac{\partial \overline{\rho u}}{\partial t} + \nabla \cdot (\overline{\rho u \otimes u} + \overline{p}\mathrm{Id} - \overline{\tau}) - \overline{\rho} g \\ = \overline{\sum_k (\rho^k u^k \otimes (w - u^k) - p^k \mathrm{Id} + \tau^k) \cdot n^k \delta_i}. \end{aligned} \tag{153}$$

The unresolved terms in Eqs. (152) and (153) can be modeled by using the one-fluid model proposed by Labourasse et al. (2007).

The momentum of the gas phase is transferred to the liquid phase in one-fluid formulation because of the continuity of velocity. Thus, kinetic energy is also transmitted to the liquid phase, which is not very significant for steady flows. Most importantly, turbulence can be carried over to the other phase through the interface. If the transition occurs from

stratified flow to stratified-wavy flow, the interfacial momentum transfer varies due to the existence of waves at the interface. This process makes modeling of the momentum transfer complicated. Therefore, two-phase flow is going to be modeled with a turbulence model by ignoring the momentum transfer and concentrate on modeling the turbulence in both phases away from the interface.

DNS is possible for single phase turbulent flow at the specified Reynolds number. It is also possible for low Reynolds number two-phase turbulent flows as well, although, it will take more time and computational effort. The turbulent two-phase stratified pipe flow problem in this thesis can be solved with DNS with the available computational resources of the Scientific Computing group of the Delft Institute for Applied Mathematics, but it will take too much time to simulate the whole computational domain. LES is feasible for both single phase and two-phase turbulent flows. In addition to this, for high Reynolds number two-phase turbulent flows, LES is the best approach for getting accurate results with less effort.

Recent studies show that LES is the most feasible candidate for modeling high Reynolds number turbulent two-phase stratified flow. On the other hand, DNS is also applicable for specific types of problems, especially for low Reynolds number flows. It gives more accurate results, which can be used to validate the simulation results with the experiment results. In order to decrease the required resources for the simulation, a method called VLES, which was proposed by Lakehal et al. (2012), can be used. This approach minimizes the modelling efforts of interface dynamics and turbulence. It is also able to predict the turbulence in large-scale and capture transient motions of interfaces.

6 The Baseline Method: Mass-Conserving Level Set (MCLS) Method

6.1 Interface Model with MCLS Method

The starting point of this thesis is a specific version of the MCLS method developed for discretization of the equations that describe immiscible incompressible two-phase flow in a circular pipe geometry. There exists complex interface topologies in between two fluids. This interface is a moving (internal) boundary. The interface can be modeled explicitly (moving mesh) or implicitly (fixed mesh) or as a combination of both. It is elaborate to simulate large numbers of different interfaces with moving meshes. Moving boundary problems can be solved with two approaches: *interface tracking* and *interface capturing*. In interface tracking, the moving boundary (interface) is described by meshes. On the other hand, in interface capturing the interface is described implicitly by an artificial scalar field.

Interface tracking methods are not applicable when there is a sharp change in the topology since the marked interface is tracked from the initial scheme, which is assumed to be not changing throughout the simulation. It is more difficult to compute the interface when it has arbitrary shape and topology. For this reason, in this study an interface capturing method is considered, which is a combination of *Level Set (LS)* and *Volume of Fluid (VOF)* methods.

In the LS method, the interface can be expressed at a given time t as the zero LS of a function called the LS function $\Phi(x,t)$. By that means, the initial surface is defined as $\{x|\ \Phi(x,0)=0\}$, $\Phi>0$ inside fluid 1 and $\Phi<0$ otherwise. The interface is shifting by the advection of Φ as a material property:

$$\frac{\partial \Phi}{\partial t} + u \cdot \nabla \Phi = 0. \tag{154}$$

The main problem with this method is that the material volume is not conserved well.

VOF defines a function, which defines the volume of a computational grid cell, and tracks the grid cells. Thereby, the fraction of each fluid phase in a grid cell is known. A marker function Ψ gives the fractional volume of specified fluid in a computational cell. For example, in a grid cell Ω, Ψ is defined by

$$\Psi = \frac{1}{vol(\Omega)} \int_{\Omega} \chi d\Omega. \tag{155}$$

where χ is the characteristic function, which has value 1 in fluid 1 and 0 elsewhere. The value of Ψ changes very fast throughout the interface because of the definition of the characteristic function. Therefore, it is difficult to compute Ψ after each transport step of the interface. Although, VOF methods are conserving mass, they are not the best choice for our problem. The reason for that is the difficulty of computing interface derivatives due to the jumps (step-like behavior) in the marker function.

Interface tracking methods mainly deal with the dynamic behavior of the interface. In addition to these methods, there exists a technique called the reconstruction of material

interfaces. This method adds discrete pieces or piecewise functions of an interface together to rebuild the continuous interface. Examples for material reconstruction are *simple line interface (SLIC)* and *piecewise linear interface construction (PLIC)*. Although, these methods are very accurate, these approaches are not considered since interface reconstruction is a difficult process.

The flow-field can be solved easily with the LS method because of the relation between the LS function Φ and interface normals, curvature and distance to the interface. However, mass is not conserved in the LS method when the interface advects. In order to conserve mass, the VOF function Ψ is used together with the LS function Φ explicitly, and this is called the *Mass-Conserving Level Set (MCLS)* method (Van der Pijl et al., 2005). The interface is assumed to be piecewise linear within a computational cell, and it is defined as:

$$\Psi = f(\Phi, \nabla\Phi). \tag{156}$$

By using Eq. (156), the advection of the interface can be computed with less effort, and Φ can be obtained directly from Ψ. The smoothing operation of Ψ is not necessary when using MCLS method. Moreover, in three-dimensional space the implementation of MCLS method is much easier than VOF method (Van der Pijl et al., 2005).

In MCLS, in order to conserve mass up to a specified tolerance, the LS function is corrected by using the fraction of Ψ in that computational cell. The fractional volume of a fluid in a given computational cell is calculated by using the LS function Φ^n; $\Psi = f(\Phi, \nabla\Phi)$.

For the first step, the LS function is advected, and re-initialization is carried out in order to smooth the function Φ. Next, Ψ evolves in time, while conserving mass, and this advected VOF function can be called as Ψ^{n+1}. Then, by using Ψ^{n+1}, Level-Set function at new time step $\Phi^{n+1,*}$ is corrected in order to find $\Psi^{n+1} = f(\Phi^{n+1}, \nabla\Phi^{n+1})$, which holds for this new Level-Set function and conserves mass (Van der Pijl et al., 2005).

6.2 Navier-Stokes Mimetic Discretization

The continuity, momentum, and energy equations are the mathematical definitions of three fundamental physical processes, and computational fluid dynamics is based on three physical principles, which are obtained by these governing equations of fluid dynamics:

- Mass is conserved,
- Momentum is conserved,
- Energy is conserved.

Model for a specific flow problem can be established by using the appropriate fundamental physical principles from above. From this model, necessary mathematical equations are defined, which express these physical principles. Therefore, our discretization technique should satisfy these principles to be able to discretize the mathematical model without loss of accuracy.

The discretization based on mimetic finite discrete first order operators (divergence, gradient, curl) mimics the properties of the original continuum differential operators; e.g.,

conservation laws, vector and tensor calculus, and fundamental identities. The Navier-Stokes equations in cylindrical coordinates possess some difficulties such as the coordinate singularity that occurs at the axis $r = 0$. In the mimetic approach, the problem near the axis is vanished by defining these discrete operators such that they mimic the properties of vector analysis in continuum case (i.e. $curl(grad) = 0$, and $div(curl) = 0$). More specifically, the discrete divergence and gradient operators are negative adjoint of each other with respect to the standard L^2 inner products. The choice of cylindrical coordinates is due to the fact that the computations become easier due to the orthogonality of the grids (Barbosa and Daube, 2005).

The properties of discrete operators in Cartesian coordinates can be analyzed, and can be realized that they also have similar definitions as already defined above in mimetic approach. For example, in Cartesian coordinates, negative of the divergence operator **-D** is the transpose of the gradient operator **G** with respect to suitable inner product if and only if particular boundary condition is satisfied. **D** and **G** operators are defined by

$$\begin{aligned} \mathbf{D} &: u \to \frac{1}{\rho}\nabla \cdot u, \\ \mathbf{G} &: \phi \to \frac{1}{\rho}\nabla\phi, \end{aligned} \tag{157}$$

where ρ is the density. Inner products of these operators yields a boundary condition as follows:

$$\int_{\partial\Omega} \phi u \cdot dS. \tag{158}$$

For velocity and pressure, the boundary condition can be written as:

$$\int_{\partial\Omega} pu \cdot dS. \tag{159}$$

For Dirichlet boundary condition, $p = 0$ at the boundary, and the integral becomes zero. For Neumann boundary condition, $u \cdot dS = u \cdot n \; dA = 0$, so the integral vanishes again.

In our approach, the discretization is carried out by using a finite difference method, which solves the incompressible Navier-Stokes equations in a cylindrical coordinate system. It is more difficult to use cylindrical coordinates, when the domain has a coordinate singularity, i.e., $r = 0$. Nevertheless, it is possible to overcome this problem by using available approaches in the literature. From those approaches, The mimetic approach is chosen for this thesis because it has some important advantages. For example, there is no need to approximate any additional term near the axis, and it is applicable everywhere in the domain (Barbosa and Daube, 2005).

Discrete spatial operators are defined such that they preserve most of the properties of the continuum operators. Mimetic finite difference operators are well-suited for this. However, they need a proper definition for inner products and discrete spaces for a proper use.

The components of discrete vector fields $\underline{\mathbf{U}}$ are defined as normal to the centers of the cell faces in the space HS. The components of $\underline{\mathbf{U}}$ are not defined at $r = 0$, and they are defined with zero normal component on the boundary. The space HS is defined as follows:

$$\mathrm{HS} = \left\{ \underline{\mathbf{U}} = \left(u_{i+1,j+1/2,k+1/2}, v_{i+1/2,j,k+1/2}, w_{i+1/2,j+1/2,k} \right) \right\}. \tag{160}$$

The inner product definition for the space HS is

$$\left(\underline{\mathbf{U}},\underline{\mathbf{U}}^{'}\right)_{\mathrm{HS}}=\sum_{i=0}^{i=I-1}\sum_{j=0}^{j=J-1}\sum_{k=0}^{k=K-1}\frac{\Delta r\Delta\theta\Delta z}{2}$$
$$[r_{i+1}u_{i+1,j+1/2,k+1/2}u^{'}_{i+1,j+1/2,k+1/2}+r_{i}u_{i,j+1/2,k+1/2}u^{'}_{i,j+1/2,k+1/2}$$
$$+r_{i+1/2}(v_{i+1/2,j+1,k+1/2}v^{'}_{i+1/2,j+1,k+1/2}+v_{i+1/2,j,k+1/2}v^{'}_{i+1/2,j,k+1/2}$$
$$+w_{i+1/2,j+1/2,k+1}w^{'}_{i+1/2,j+1/2,k+1}+w_{i+1/2,j+1/2,k}w^{'}_{i+1/2,j+1/2,k})]. \quad (161)$$

where $\Delta r = 1/I$, $\Delta\theta = 2\pi/J$, and $\Delta z = H/K$ are the increments of staggered uniform grid in the discretized computational domain. The discrete scalar function $\boldsymbol{\phi}$ is defined at the cell centers in the space HC:

$$\mathrm{HC}=\boldsymbol{\phi}=(\phi_{i+1/2,j+1/2,k+1/2}). \quad (162)$$

The space HC has the following inner product:

$$\left(\boldsymbol{\phi},\boldsymbol{\phi}^{'}\right)_{\mathrm{HC}}=\sum_{i=1}^{i=I}\sum_{j=1}^{j=J}\sum_{k=1}^{k=K}\phi_{i-1/2,j-1/2,k-1/2}\phi^{'}_{i-1/2,j-1/2,k-1/2}r_{i-1/2}\Delta r\Delta\theta\Delta z. \quad (163)$$

The discrete vector fields $\underline{\mathbf{V}}$ is defined at the mid edges of the cells in the space HL:

$$\mathrm{HL}=\{\mathbf{V}=(\eta_{i+1/2,j,k},\omega_{i,j+1/2,k},\zeta_{i,j,k+1/2})\}. \quad (164)$$

The discrete scalar function $\boldsymbol{\psi}$ is defined at the vertices (i,j,k) of the cells in the space HN:

$$\mathrm{HN}=\{\boldsymbol{\psi}=(\psi_{i,j,k})\}. \quad (165)$$

The gradient operator is defined as the negative adjoint of the discrete divergence operator with respect to the given inner products:

$$(\boldsymbol{\phi},\overline{\mathbf{D}}_S(\underline{\mathbf{U}}))_{\mathrm{HC}}=-(\overline{\mathrm{G}}(\boldsymbol{\phi},\overline{\mathbf{U}})_{\mathrm{HS}}, \quad (166)$$

where the gradient operator $\overline{\mathrm{G}}$ maps HC onto HS, and the divergence operator $\overline{\mathbf{D}}_S$ maps HS onto HC. The curl operator $\overline{\mathbf{C}}_S$ maps HS onto HL, where discrete vorticity components are defined at the edge centers (Barbosa and Daube, 2005). The usual properties of vector analysis such as $curl(grad) = 0$ and $div(curl) = 0$ can be checked with the given discrete operators;

$$\overline{\mathbf{C}}_S(\overline{\mathrm{G}}(\boldsymbol{\phi}))=0 \quad \forall\boldsymbol{\phi}\ \text{in HC}, \quad (167)$$

$$\overline{\mathbf{D}}_L(\overline{\mathbf{C}}_S(\underline{\mathbf{U}}))=0 \quad \forall\underline{\mathbf{U}}\ \text{in HS}, \quad (168)$$

where $\overline{\mathbf{D}}_L$ is the divergence operator, which is a mapping from HL onto HN.

Artificial sources of energy and vorticity may lead to unphysical long terms in LES. Above all, mimetic schemes are useful for LES because of vorticity preserving discretizations. When a mimetic curl operator is applied to the discrete momentum equation, a consistent discrete vorticity equation is obtained, which is called the vorticity preservation (Abba and Bonaventura, 2008).

The formulation as is currently used assumes a constant viscosity. If this method is to be used in combination with a LES model, then the formulation has to be extended (subgrid

scale model) to allow for a variable viscosity. Otherwise, it is not possible to simulate the problem. Also, a boundary condition that allows to solve for the pressure difference over the pipe as part of the problem needs to be implemented for DNS. For that reason, a velocity flow rate needs to be specified using velocity profiles, inflow and outflow pressures.

7 Conclusions and Future Plans

In this study, modeling of immiscible incompressible turbulent two-phase stratified flow is investigated. The most appropriate turbulent model for this type of pipe flow is identified by getting more insight into the current state-of-the-art of modeling of turbulent two-phase stratified flow. The experiments, which have been carried out in the Laboratory for Aero- and Hydrodynamics of Faculty of Mechanical, Maritime and Materials Engineering of Delft University of Technology, are used as a reference in order to to validate the results of this study.

Modeling of multiphase turbulent flows compared to single-phase turbulent flows with high accuracy is more difficult. Although, the interface between two immiscible phases can be described quite precisely with available methods, the influence of the turbulent fluctuations in one of the phases may have great influence on the dynamics of the interface. Thus, it is very important to clarify the effect of the turbulence in all phases. There are considerably few studies about turbulence model of two-phase stratified pipe flow. In addition to this, LES is not the common practice in turbulent two-phase stratified pipe flow. Therefore, in order to have an idea about the flow properties (e.g., velocity profile), first, DNS and LES methods are used for single-phase turbulent pipe flow, then, necessary inferences are made about two-phase turbulent pipe flow.

The grid estimations for DNS and LES are calculated and compared in order to find the most appropriate model, which predicts the onset of instability of the interface and the formation of slugs. By estimating the number of total grid points required for the single-phase turbulent flow, which gives a rough estimate of how many unknowns are there, a minimum requirement and an inference about the complexity of the two-phase flow are acquired. The estimations for grid resolution that are carried out in this thesis are compared to DNS results of Eggels (1994), which was measured for single-phase flow at $Re_\tau = u_\tau D/\nu_\tau = 360$ (close to the value used in this thesis $Re_\tau = 395$). The results of the grid estimation is validated by first checking it on the case of Eggels (1994), then adapting the procedure to the problem case described in this thesis (see Appendices A and B).

The comparison of computational costs revealed that DNS is also feasible for this pipe flow problem. LES of turbulent two-phase flow is more feasible than DNS, but the computational effort by doing LES is not significantly decreased. The reason behind that is the small value of the Reynolds number, which is not in the optimum range for doing LES. Another reason is that the boundary layer thickness is also quiet large for that Reynolds number, which results in unrealistic grid-point estimation for LES with uniform grid spacing. The results of estimating the required number of grid-points for single-phase flow yield that both DNS and LES are possible for the given case. However, LES and RANS (without any limitation) are on the safe side, but DNS is just within the limits of available computational power. Therefore, DNS and LES are considered to be the main consideration for the future plan of the research. For that reason, in order to accomplish this future plan a variable viscosity is defined for the discretization method together with the LES model. Also, a boundary condition that allows to solve for the pressure difference over the pipe as part of the problem needs to be implemented for DNS.

The first plan for the research is to simulate single-phase pipe flow problem of Eggels (1994) with DNS (or with LES). Afterward, the results of the simulation will be validated

with the study of Eggels (1994). Subsequently, the same approach will be implemented in this thesis and it is going to be validated by comparing with the results of the experiment that has been carried out in the Laboratory for Aero- and Hydrodynamics of Faculty of Mechanical, Maritime and Materials Engineering of Delft University of Technology. Thereafter, immiscible incompressible turbulent two-phase stratified pipe flow problem will be simulated with DNS, and with LES. For this part, the effect of the momentum transfer between two phases will be neglected in order to make the problem slightly easier. The final goal is to predict the formation of slugs using VLES as suggested by Lakehal et al. (2012) if only there will be enough time.

Appendices

A Estimating Computational Cost for DNS

First, the estimation procedure, which has been carried out in the study of Eggels (1994) for the total number of grid points is validated in this thesis for $Re_\tau = 395$. The following relations have been defined in the work of Eggels (1994):

$$L = 5D, \quad \tilde{L} = 5, \tag{169}$$

$$\tilde{l} = \frac{1}{10}\tilde{L} = 0.5, \tag{170}$$

where L is the pipe length, D is the diameter of the pipe, l is the largest length scale and the tilde symbol ˜ indicates a normalization in terms of the characteristic length scale (e.g., pipe diameter).

In the study, DNS has been carried out using $96 \times 128 \times 256$ grid points *equally* spaced in r-, θ-, and z-direction respectively. The grid spacing has been computed as $\Delta r^+ \approx 1.88$, $\Delta z^+ \approx 7.03$ in terms of viscous wall units [8]. The azimuthal grid spacing varies linearly with r and it has its minimum value $(\Delta r \Delta\theta/2)^+ \approx 0.05$ near the centerline of the pipe and its maximum value $(D\Delta\theta/2)^+ \approx 8.84$ at the wall [9].

The dimensionless grid spacing in r-direction is equal to

$$\tilde{h_r} = \frac{\Delta r}{D} = \frac{1}{2N_r}. \tag{171}$$

The number of grid points in r-direction is $N_r = 96$. Therefore,

$$\tilde{h_r} = \frac{1}{2(96)} \approx 0.0052. \tag{172}$$

Furthermore, the dimensionless grid spacing h_r (with respect to the pipe diameter) can be also calculated with the following approach (where $y^+ = 1$), which is in agreement with the study:

$$\tilde{h_r} = \frac{\Delta r}{D} = 2(y^+)\sqrt{74}(Re_D^{-13/14}) = 2\sqrt{74}(5300^{-13/14}) \approx 0.0059, \tag{173}$$

where the Reynolds number with the bulk velocity is $Re_D = 5300$.

The dimensionless grid spacing in θ-direction can be calculated as follows:

$$\tilde{h_\theta} = \frac{\Delta\theta}{2} = \frac{2\pi}{2N_\theta} = \frac{\pi}{128} \approx 0.0245, \tag{174}$$

where the number of grid points in θ-direction is $N_\theta = 128$. It can be seen that the ratio of the dimensionless grid spacing in θ-direction and dimensionless grid spacing in r-direction

[8] A superscript $^+$ corresponds to a normalization in terms of viscous wall units

[9] The maximum value of the grid spacing in θ-direction is calculated by assuming $D - \Delta r \approx D$ (subtracting Δr from the pipe diameter represents distance of the center point of the last grid cell to the center of the pipe), and for the minimum value of the grid spacing, the distance of the first grid cell to the center of the pipe is $\Delta r/2$.

is $\tilde{h_\theta}/\tilde{h_r} \approx 4.7$. Moreover, the ratio of grid spacings computed in the study of Eggels (1994) also has the same ratio $(D\Delta\theta/2)^+/\Delta r^+ \approx 4.7$

The total number of grid points in the z-direction is $N_z = 256$:

$$N_z = 256 = \frac{\tilde{L}}{\tilde{h_z}}, \tag{175}$$

where $\tilde{h_z}$ is the dimensionless grid spacing in z-direction, and is equal to

$$\tilde{h_z} = \frac{\tilde{L}}{N_z} = \frac{5}{256} \approx 0.0195. \tag{176}$$

The ratio of the dimensionless largest length scale to the dimensionless grid spacing in z-direction is $\tilde{l}/\tilde{h_z} = 0.5/0.0195 \approx 25.6$. The ratio of dimensionless grid spacing in z-direction and dimensionless grid spacing in r-direction is $\tilde{h_z}/\tilde{h_r} = 0.0195/0.0052 \approx 3.75$, which is almost same as the ratio given by the study $\Delta z^+/\Delta r^+ = 7.03/1.88 \approx 3.74$.

The same approach is implemented in this thesis. However, the Reynolds number Re_D computed with bulk velocity and characteristic length (in this case it is the pipe diameter) has a different value, $Re_D = 3421$. Therefore, the dimensionless grid spacing in r-direction $\tilde{h_r}$ (with respect to the pipe diameter, and $y^+ = 1$) is

$$\tilde{h_r} = \frac{\Delta r}{D} = 2(y^+)\sqrt{74}(Re_D^{-13/14}) = 2\sqrt{74}(3421^{-13/14}) \approx 0.0089. \tag{177}$$

Hence, the number of grid points in r-direction is

$$N_r = \frac{1}{2\tilde{h_r}} = \frac{1}{2(0.0089)} \approx 56. \tag{178}$$

If the same relation between dimensionless grid spacings are used, i.e., $\tilde{h_z}/\tilde{h_r} \approx 3.75$, and $\tilde{h_\theta}/\tilde{h_r} \approx 4.7$, then $\tilde{h_z} \approx 0.0333$, and $\tilde{h_\theta} \approx 0.0418$. In this way, the number of grid points required in θ- and z-direction can be calculated respectively:

$$N_\theta = \frac{\pi}{\tilde{h_\theta}} = \frac{\pi}{0.0418} \approx 75, \tag{179}$$

$$N_z = \frac{\tilde{L}}{\tilde{h_z}} = \frac{50}{0.0333} \approx 1501, \tag{180}$$

where the length of the pipe is taken as one-fourth of the whole length of the pipe, i.e., $L = 50D$, thereby, the dimensionless pipe length with respect to the pipe diameter is $\tilde{L} = L/D = 50$. According to the study of Eggels (1994), the two-point correlation coefficients get small enough around $L = 2.5D$. If we choose our computational domain length L equal to $2.5D$, then the dimensionless length scale with respect to the diameter is $\tilde{L} = 2.5$, which yields

$$N_z = \frac{\tilde{L}}{\tilde{h_z}} = \frac{2.5}{0.0333} \approx 75. \tag{181}$$

The uniform grid spacing approach above mimics the estimation procedure that has used in the work of Eggels (1994). The DNS approach below is carried out (without reverse engineering the study of Eggels (1994)) with non-uniform grid spacing in r-direction, and

uniform grid spacing in θ- and z-direction. The radial grid spacing has a minimum value $\Delta r^+ \approx 1$ near the pipe wall and reaches a maximum value $\Delta r^+ \approx 5$ near the centerline of the pipe. The azimuthal grid spacing varies linearly with r and reaches a minimum value $(\Delta r \Delta\theta/2)^+ \approx 0.0258$ near the centerline of the pipe and its maximum value $(D\Delta\theta/2)^+ \approx 5$ at the pipe wall.The grid spacing in axial direction $\Delta z^+ \approx 10$.

In order not to exceed the available computational power (i.e., $30\times150\times90$), the number of grid points and the aspect ratio for the grid spacing in r-direction is selected accordingly. The number of grids in θ-direction is calculated as follows:

$$(D\Delta\theta/2)^+ = (r\Delta\theta)^+ = \left(r\frac{2\pi}{N_\theta}\right)^+ \approx 5 \quad \rightarrow \quad N_\theta \approx 248. \tag{182}$$

The number of grids in z-direction is calculated as follows:

$$(\Delta z)^+ = \frac{L}{N_z} \approx 10 \quad \rightarrow \quad N_z \approx 198, \tag{183}$$

where $L = 5D$ and $D = 395$ in dimensionless wall units. Thus, the number of grid points required for DNS is $11\times248\times198$, and the aspect ratio is $n = 1.16613$ for the non-uniform grid spacing in r-direction. The maximum available computational power is actually exceeded (approximately 20%) with these number of grid points.

B Estimating Computational Cost for LES

The characteristic grid spacing Δ_{ch} is calculated from the grid spacing in all three directions:

$$\Delta_{ch} = \sqrt{\frac{\Delta r^2 + r^2\Delta\theta^2 + \Delta z^2}{3}}, \tag{184}$$

where Δr, $r\Delta\theta$, and Δz are the grid spacings in radial, tangential, and axial direction respectively. The ratio of l_{mix} [10] and Δ_{ch} is denoted by the Smagorinsky coefficient c_s, which is a measure for the numerical resolution, as:

$$c_s = \frac{l_{mix}}{\Delta_{ch}}. \tag{185}$$

Values of c_s less than 0.165 give insufficient spatial resolution (Eggels, 1994). Moreover, the ratio of l_{mix} and the filter length Δ:

$$\frac{l_{mix}}{\Delta} = \frac{(\frac{3}{2}\alpha_K)^{-3/4}}{2\pi} = 0.0825, \tag{186}$$

where α_K is the Kolmogorov constant and equals approximately 1.6. Hence, if the same relation holds for the filtering length and characteristic grid spacing $\Delta \geq 2\Delta_{ch}$ (see Eq. (99)), then the following relation is obtained for the mixing length of the SGS motions:

$$l_{mix} = 0.0825\Delta \quad \rightarrow \quad \frac{l_{mix}}{\Delta_{ch}} = c_s \geq 0.165. \tag{187}$$

In the work of Eggels (1994), the value chosen for c_s is approximately 0.1, which is less than 0.165. The reason for using smaller value is that larger values of c_s does not maintain resolved scale motions and it gives unrealistic results in the end. The value of c_s is dependent on the type of flow in terms of the way how turbulence is produced. In order to obtain the number of grids required in LES, the Eq. (187) substituted into the Eq. (99) (Δ_x has been replaced by Δ_{ch}):

$$N_L = \frac{L}{l}\frac{l}{\Delta}\frac{\Delta}{\Delta_{ch}} = \frac{L}{l}\frac{l}{\Delta}\frac{c_s}{0.0825}. \tag{188}$$

The following relation is obtained by approximating $L/l \approx 10$ and $c_s \approx 0.1$ for shear-driven turbulent flow:

$$N_L \approx 12\frac{l}{\Delta}. \tag{189}$$

In the study, equally spaced $16 \times 64 \times 128$ grid points (N_r, N_θ, and N_z) have been used for three cases, and the viscous wall layer has not been resolved in these cases. Therefore, the first grid-point is located within the inertial sublayer (i.e., $y^+_{min} = 32.8 > 30$). The grid spacing in r, θ, and z-direction are $\Delta r^+ = 65.6$, $(D\Delta\theta/2)^+ = 103.1$, and $\Delta z^+ = 82.0$ respectively.

The dimensionless mesh width (with respect to the pipe diameter) in r-direction can be calculated as follows:

$$\tilde{h_r} = \frac{1}{2N_r} = \frac{1}{32} \approx 0.0312. \tag{190}$$

[10] The length scale l_{mix} represents the mixing length of the SGS motions.

The value above can be validated by using Eq. (177) with $y^+ = 32.8$:

$$\tilde{h_r} = \frac{\Delta r}{D} = 2(y^+)\sqrt{74}(Re_D^{-13/14}) = 2(32.8)\sqrt{74}(40000^{-13/14}) \approx 0.0301. \tag{191}$$

With the same approach the dimensionless mesh width in θ- and z-direction is calculated:

$$\tilde{h_\theta} = \frac{\Delta\theta}{2} = \frac{\pi}{N_\theta}\frac{\pi}{64} \approx 0.0490, \tag{192}$$

$$\tilde{h_z} = \frac{\tilde{L}}{N_z} = \frac{5}{128} \approx 0.0390. \tag{193}$$

The ratio of $\tilde{h_z}$ and $\tilde{h_r}$ equals to 1.25, which can be validated by taking the ratio of $\Delta z^+/\Delta r^+ \approx 1.25$. Moreover, the ratio of $\tilde{h_\theta}$ and $\tilde{h_r}$ approximately equals to 1.57. This ratio can also be validated by taking the ratio of $(D\Delta\theta/2)^+$ and Δr^+, which is also around 1.57.

In this thesis, the dimensionless mesh width in r-direction is calculated in Eq. (177) with $y^+ = 1$. For $y^+ = 32.8$, the dimensionless mesh width in r-direction is

$$\tilde{h_r} = \frac{\Delta r}{D} = 2(y^+)\sqrt{74}(Re_D^{-13/14}) = 2(32.8)\sqrt{74}(3421^{-13/14}) \approx 0.2919. \tag{194}$$

Thus, the number of grid points in r-direction is

$$N_r = \frac{1}{2\tilde{h_r}} = \frac{1}{0.5838} \approx 2 \tag{195}$$

It can be concluded that the boundary layer modeling is not feasible for this case since the Reynolds number is not large enough and the modeled boundary layer (viscous wall region) is almost equal to the radius of the pipe diameter. For other directions, the same approach can be implemented by using the ratios:

$$\tilde{h_\theta} = 1.57\tilde{h_r} \approx 0.4582, \tag{196}$$

$$\tilde{h_z} = 1.25\tilde{h_r} \approx 0.3648. \tag{197}$$

The number of grid points in θ- and z-direction can be calculated as follows:

$$N_\theta = \frac{\pi}{\tilde{h_\theta}} = \frac{\pi}{0.4582} \approx 7, \tag{198}$$

$$N_z = \frac{\tilde{L}}{\tilde{h_z}} = \frac{50}{0.3648} \approx 137, \tag{199}$$

where $\tilde{L} = 50$. For $\tilde{L} = 2.5$, the number of grid points in z-direction is

$$N_z = \frac{\tilde{L}}{\tilde{h_z}} = \frac{2.5}{0.3648} \approx 7. \tag{200}$$

The other computation case in the work of Eggels (1994) has been carried out using 32×128×192 grid points with *non-uniform* grid spacing only in r-direction (*uniform* grid

spacing in other directions). The value of the dimensionless wall unit for these computations is $y^+ = 1.5$. The averaged value for the grid spacing in r-direction is $(\Delta r^+)^* = 32.8$, and for other directions the values are $(D\Delta\theta/2)^+ = 51.5$, $\Delta_z^+ = 54.7$.

The aspect ratio used in the non-uniform cases can be evaluated. In order to do that, first, the total sum of each grid spacings in r-direction should be computed as follows:

$$(\Delta r^+)^* = \frac{\sum_i \Delta r_i^+}{N_r}, \quad \rightarrow \quad \sum_i \Delta r_i^+ = (\Delta r^+)^*(N_r) = (32.8)(32) = 1049.6. \tag{201}$$

The value for the aspect ratio with the calculated total sum of grid spacings is approximately equals to 1.16613. The same aspect ratio is used in this thesis as well, and the number of grid points needed in r-direction can be calculated by using the same value for the aspect ratio. The first grid-point is at $\tilde{h_{r1}} = 0.0135$ for $y^+ = 1.5$. The number of grid points required in r-direction is $N_r = 16$, which is calculated by using the aspect ratio and the first grid spacing $\tilde{h_{r1}}$.

The ratio of the grid spacing in θ-direction to r-direction is $(D\Delta\theta/2)^+/(\Delta r^+)^* \approx 1.5701$. Therefore, the grid spacing in θ-direction is

$$\tilde{h_\theta} = (1.5701)(\tilde{h_r})^* = (1.5701)(0.0625) \approx 0.0981, \tag{202}$$

where $(\tilde{h_r})^*$ is the averaged grid spacing in r-direction. Therefore, the number of grid points required in θ-direction is $N_\theta = 32$.

The ratio of the grid spacing in z-direction to r-direction is $\Delta z^+/(\Delta r^+)^* \approx 1.6676$. Thus, the grid spacing in z-direction is

$$\tilde{h_z} = (1.6676)(\tilde{h_r})^* = (1.6676)(0.0625) \approx 0.1042. \tag{203}$$

Hence, the number of grid points required in z-direction is $N_z = 480$ for $\tilde{L} = 50$, and for $\tilde{L} = 2.5$, the number of grid points required in z-direction is $N_z = 24$.

References

Abba, A. and Bonaventura, L. (2008). A mimetic finite difference discretization for the incompressible navier-stokes equations. *International Journal for Numerical Methods in Fluids*, 56(8):1101.

Absi, R. (2009). A simple eddy viscosity formulation for turbulent boundary layers near smooth walls. *Comptes Rendus Mecanique*, 337(3):158–165.

Avila, M. (2015). Lecture notes in Reynolds averaged Navier-Stokes (RANS).

Bakker, A. (2005). Lecture notes in turbulence models.

Barbosa, E. and Daube, O. (2005). A finite difference method for 3D incompressible flows in cylindrical coordinates. *Computers & Fluids*, 34(8):950–971.

Berthelsen, P. A. and Ytrehus, T. (2005). Calculations of stratified wavy two-phase flow in pipes. *International Journal of Multiphase Flow*, 31(5):571–592.

Birvalski, M. (2015). *Experiments in stratified gas-liquid pipe flow*. TU Delft, Delft University of Technology.

Boersma, B. and Nieuwstadt, F. (1996). Large-eddy simulation of turbulent flow in a curved pipe. *Journal of Fluids Engineering*, 118(2):248–254.

Chinello, G. (2015). CFD modelling of stratified two-phase flow for oil and gas transportation. Master's thesis.

Eggels, J. and Nieuwstadt, F. (1993). Large eddy simulation of turbulent flow in an axially rotating pipe. In *Proceeding of the 9th Symposium on Turbulent Shear flows*, pages 310–1.

Eggels, J., Unger, F., Weiss, M., Westerweel, J., Adrian, R., Friedrich, R., and Nieuwstadt, F. (1994). Fully developed turbulent pipe flow: a comparison between direct numerical simulation and experiment. *Journal of Fluid Mechanics*, 268:175–210.

Eggels, J. G. M. (1994). *Direct and large eddy simulation of turbulent flow in a cylindrical pipe geometry*. TU Delft, Delft University of Technology.

Frank, T. (2003). Numerical simulations of multiphase flows using CFX-5. In *CFX Users conference, Garmisch-Partenkirchen, Germany*.

Fu, S., Launder, B., and Leschziner, M. (1987). Modelling strongly swirling recirculating jet flow with reynolds-stress transport closures. In *6th Symposium on Turbulent Shear Flows*, pages 17–6.

Fulgosi, M., Lakehal, D., Banerjee, S., and De Angelis, V. (2003). Direct numerical simulation of turbulence in a sheared air–water flow with a deformable interface. *Journal of Fluid Mechanics*, 482:319–345.

George, W. K. (2013). Lecture notes in turbulence for the 21st century.

Ghorai, S. and Nigam, K. (2006). CFD modeling of flow profiles and interfacial phenomena in two-phase flow in pipes. *Chemical Engineering and Processing: Process Intensification*, 45(1):55–65.

Gibson, M. and Launder, B. (1978). Ground effects on pressure fluctuations in the atmospheric boundary layer. *Journal of Fluid Mechanics*, 86(03):491–511.

Gnambode, P., Orlandi, P., Ould-Rouiss, M., and Nicolas, X. (2015). Large-eddy simulation of turbulent pipe flow of power-law fluids. *International Journal of Heat and Fluid Flow*, 54:196–210.

Kataoka, I. (1986). Local instant formulation of two-phase flow. *International Journal of Multiphase Flow*, 12(5):745–758.

Labourasse, E., Lacanette, D., Toutant, A., Lubin, P., Vincent, S., Lebaigue, O., Caltagirone, J.-P., and Sagaut, P. (2007). Towards large eddy simulation of isothermal two-phase flows: Governing equations and a priori tests. *International Journal of Multiphase Flow*, 33(1):1–39.

Lakehal, D., Labois, M., and Narayanan, C. (2012). Advances in the large–eddy and interface simulation (leis) of interfacial multiphase flows in pipes. *Progress in Computational Fluid Dynamics, an International Journal*, 12(2-3):153–163.

Lakehal, D., Laboisa, M., Caviezela, D., and Belhouachib, B. (2011). Transition of gas-liquid stratified flow in oil transport pipes. *J. Eng. Res*, 8(2):49–58.

Lamarque, N., Zoppé, B., Lebaigue, O., Dolias, Y., Bertrand, M., and Ducros, F. (2010). Large-eddy simulation of the turbulent free-surface flow in an unbaffled stirred tank reactor. *Chemical Engineering Science*, 65(15):4307–4322.

Lombardi, P., De Angelis, V., and Banerjee, S. (1996). Direct numerical simulation of near-interface turbulence in coupled gas-liquid flow. *Physics of Fluids (1994-present)*, 8(6):1643–1665.

McDonough, J. M. (2007). Lecture notes in introductory lectures on turbulence.

Pope, S. B. (2001). *Turbulent flows*. IOP Publishing.

Prosperetti, A. and Tryggvason, G. (2009). *Computational methods for multiphase flow*. Cambridge university press.

Saad, T. (2011). Lecture notes in turbulence modeling for beginners.

Sondak, D. L. (1992). Wall functions for the k-ϵ turbulence model in generalized nonorthogonal curvilinear coordinates.

Ullmann, A. and Brauner, N. (2006). Closure relations for two-fluid models for two-phase stratified smooth and stratified wavy flows. *International Journal of Multiphase Flow*, 32(1):82–105.

Vallée, C., Höhne, T., Prasser, H.-M., and Sühnel, T. (2008). Experimental investigation and CFD simulation of horizontal stratified two-phase flow phenomena. *Nuclear Engineering and Design*, 238(3):637–646.

Van der Pijl, S., Segal, A., Vuik, C., and Wesseling, P. (2005). A mass-conserving level-set method for modelling of multi-phase flows. *International Journal for Numerical Methods in Fluids*, 47(4):339–361.

Vijiapurapu, S. and Cui, J. (2010). Performance of turbulence models for flows through rough pipes. *Applied Mathematical Modelling*, 34(6):1458–1466.

Wilcox, D. C. et al. (1998). *Turbulence modeling for CFD*, volume 2. DCW industries La Canada, CA.

Wörner, M. (2003). *A compact introduction to the numerical modeling of multiphase flows*. Forschungszentrum Karlsruhe.